JOINT CHANNEL ESTIMATION AND OFDM SYNCHRONIZATION IN MULTIPATH FADING

LIM WEI CHEE

NATIONAL UNIVERSITY OF SINGAPORE

2004

JOINT CHANNEL ESTIMATION AND OFDM SYNCHRONIZATION IN MULTIPATH FADING

LIM WEI CHEE

(B. Eng. (Hons.), NUS)

A THESIS SUBMITTED

FOR THE DEGREE OF MASTER OF ENGINEERING

DEPARTMENT OF

ELECTRICAL AND COMPUTER ENGINEERING

NATIONAL UNIVERSITY OF SINGAPORE

2004

Acknowledgment

I would like to express my warmest thanks to those who have consistently been helping me with my research work.

I am grateful to my supervisors, Prof. Tjhung Tjeng Thiang and Dr Balakrishnan Kannan, for their encouragement, support and valuable advice on my research work, all along the way of improving both my skills in research and my attitude to overcome problems.

I want to thank sincerely all my colleagues and friends in I2R for providing a great environment to work in.

Last but not least, I must thank my family for their support, love and care, which I can never live without.

Contents

Summary

Orthogonal frequency division multiplexing (OFDM) modulation technique is known to be robust against inter-symbol interference (ISI) resulting from multipath propagation, which is one of the limiting factors when wideband data is transferred over a wireless medium. However studies have shown that the transmission performance of OFDM is very sensitive to inaccurate frequency and time references. A carrier offset at the receiver can cause loss in subcarrier orthogonality and thus introduce inter-carrier interference (ICI) that severely degrades system performance, while timing offset causes ISI as the demodulating FFT window will spill over to the next symbol. Accurate carrier and timing offset estimation and compensation are important in OFDM communications. Moreover, in order to achieve coherent demodulation, channel gains need to be estimated. Hence effective joint channel estimation and synchronization is of paramount importance in OFDM and is the focus of this thesis. An OFDM framework complying with the IEEE 802.11a Wireless LAN standards is considered. The effects of both timing and frequency offset were first examined. We then present an algorithm to estimate the channel, timing and frequency offset simultaneously in the time domain by using a maximum-likelihood technique. We consider both acqui-

sition and tracking. In the acquisition stage, we first derived a maximum likelihood estimation solution for channel coefficients which turns out to be a correlator. Then, we proved that it is possible to extract the timing and frequency offset from the channel estimate. Using the estimates obtained from the acquisition, we then fine-tune our estimates in the tracking stage to achieve better performance. Furthermore, our algorithm is much simpler, more robust, accurate and reliable than existing joint estimation techniques because we avoided the need of a coarse synchronization algorithm.

List of Figures

List of Tables

Chapter 1

Introduction

1.1 Background

The increasing demand for wireless multimedia and future-generation mobile communication services has led to intense interest in modulation techniques that can provide broadband transmission over wireless channels. Bandwidth efficiency is one of the most important criteria in the design of a communication system. The designer must decide how to efficiently utilize the available channel bandwidth in the order to transmit the information reliably within the transmission power and receiver complexity constraints.

For high-speed data transmission over mobile radio channels, multipath propagation is predominant and it causes Inter-Symbol Interference (ISI). This is a major obstacle to overcome as it causes bit errors at the receiver and results in the degradation in performance of a communication system. The degree of degradation is dependent on the frequency response characteristics

1

of the channel.

For communication in a mobile radio channel, one approach is to employ a single carrier system in which the information sequence is transmitted serially at some specified rate. In such a channel, the time dispersion is generally much greater than the symbol duration, resulting in ISI. In this case, an equaliser, at the cost of increased receiver complexity, is necessary to compensate for the channel distortion.

An alternate approach is multicarrier modulation, which is based on the concept of channel partitioning, in which we divide a wideband, frequency selective channel into a number of parallel narrowband sub-channels. The bandwidth of each sub-channel is set sufficiently small so that the channel frequency response is almost constant within the sub-channel. Instead of having a single carrier being modulated by a single data stream, multiple carriers, each simultaneously modulated by a much lower rate data stream, are employed in a multicarrier system. That is in multicarrier system, the high rate data is split into many slower rate data and are transmitted in parallel. Equalization is no longer necessary to remove ISI, as it is negligible. Theoretically speaking, multicarrier techniques can yield transmission rates close to the channel capacity [2].

1.2 OFDM

1.2.1 Introduction

Orthogonal Frequency Division Multiplexing (OFDM) is a multicarrier modulation technique whose fundamental principle originates from Chang [3] and over the years a number of researchers have investigated this technique [4–6].

In contrast with the conventional Frequency Division Multiplexing (FDM), the spectrum of the individual carriers in an OFDM symbols are allowed to mutually overlap, therefore giving optimum spectrum efficiency. In order to maintain orthogonality of the carriers on a symbol interval, the carriers must be synthesized in a manner such that they are spaced in frequency at exactly the reciprocal of the symbol interval, i.e. $\frac{1}{T_s}$. Such synthesis can be accomplished perfectly in principle by using the discrete fourier transform (DFT). In such a scheme, the serial data stream is first split into N streams via a serial to parallel converter. An N-point IDFT is then performed to generate the baseband samples to be transmitted.

1.2.2 Applications of OFDM

The recent evolution of integrated circuit digital signal processing chips has made it practical to implement OFDM for high-speed data transfer applications. The recent successful applications in OFDM include:

1. Digital Audio Broadcasting (DAB) [7]

Standardized by European Technical Standards Institute (ETSI) in 1995, Digital Audio Broadcasting (DAB) was the first standard to use OFDM. DAB makes a single frequency network and the efficient handling of multipath delay spread resulting in improved CD quiality sound, new data services and higher spectrum efficiency.

2. Terrestrial Digital Video Broadcasting [8]

A personal area network (PAN) broadcasting industry group created Digital Video Broadcasting (DVB) in 1993. DVB produces a set of specifications for the delivery of digital television over cable, DFL and satellite. in 1997 the terrestrial network, Digital Terrestrial Television Broadcasting (DTTB), was standardized. DTTB utulizes OFDM in the 2000 and 8000 sub-carrier modes.

3. Magic WAND

The Magic Wireless ATM network Demonstrator (WAND) was a result of the European Advanced Communications Technology and Server (ACTS) program. A prototype of a wireless OFDM based ATM network was implemented by Magic WAND. This prototype largely impacted standards activities in the 5GHz band as a result of employing OFDM based modems and gaining acceptance for OFDM in high-rate wireless communications and forming the basis for HiperLAN2.

4. IEEE 802.11a/HiperLAN2 and MMAC Wireless LAN [9]

OFDM in the new 5GHz band is comprised of 802.11a, HiperLAN2 and WLAN standards. In July 1998, IEEE selected OFDM as the basis for the new 802.11a 5GHz standard in the U.S. targeting a range of data

rates up to 54 Mbps. In Europe, ETSI project Broadband Radio Access Networks (BRAN) is now working on three extensions for OFDM in the HiperLAN standard:

(a) HiperLAN2, a wireless indoor LAN with a Qos provision;

(b) Hiperlink, a wireless indoor backbone; and

(c) HiperAccess, an outdoor, fixed wireless network providing access to a wired infrastructure.

In Japan, consumer electronics companies and service providers are cooperating in the MMAC project to define new wireless standards similar to those of IEEE and ETSI BRAN.

1.2.3 Advantages and disadvantages of OFDM

Advantages

In an OFDM system, orthogonality between the sub-carriers results in high spectral efficiency. With its parallel transmission scheme, a wideband high data rate stream is converted into multiple narrowband, lower bit rate streams. In high data rate serial transmission, a deep fade in a mobile channel causes burst errors. In contrast, each OFDM symbol generally has a duration that is much longer than the coherence time of the channel. As a result, there is only slight distortion to the many data symbols which are time interleaved in an OFDM symbol. Hence, the data symbols may still be correctly demodulated. The multicarrier nature of OFDM also allows transmission of the same

information bearing signal in many different carriers, permitting frequency diversity [10,11]. In addition to this, the availability of inexpensive DSP and VLSI technologies has made implementation of OFDM systems practical and flexible.

Disadvatages

Before demodulation of subcarriers can take place, an OFDM receiver has to perform at least 2 synchronization tasks. Firstly, the symbol timing boundaries have to be determined to minimize the effects of ISI. Secondly, it has to estimate and compensate for the carrier frequency offset of the received signal with respect to the receiver because such an offset will destroy the orthogonality between the subcarriers and introduces inter-carrier interference (ICI). A related problem is phase noise, since a practical oscillator produces a carrier that is phase modulated by the random phase jitter. As a result, the frequency, which is the time derivative of the phase, is never perfectly constant, thereby causing ICI in an OFDM receiver. For single carrier systems, phase noise and frequency offsets only degrades the received signal -to-noise ratio (SNR), rather than introducing interference. This is the reason that the sensitivity to phase noise and frequency offset are often mentioned as disadvantages of OFDM relative to single carrier systems. An OFDM signal consists of a number of independently modulated subcarriers that can result in a large peak-to-average power ratio (PAPR) when added up coherently. When N_s signals are added with the same phase, they produce a peak power that is N_s times the average power. High PAPR is also a major problem in

OFDM as a large PAPR increases the complexity of the analogue-to-digital and digital-to-analogue converters and reduces the efficiency of the RF power amplifier employed in the system. Moreover, in order to achieve coherent demodulation, channel gains need to be estimated.

1.3 Thesis Organization

The organization of this thesis is as follows:

Chapter 1 - The concept of OFDM is introduced together with the critical problem of joint channel estimation and timing synchronization and carrier frequency offset estimation. A review of the available techniques follow and an account of the thesis outline and contribution is given.

Chapter 2 - The signal model for a general OFDM system used in this thesis is formulated. The OFDM packet used in IEEE 802.11a wireless LAN standard is described in detail. A brief introduction of wireless communications channel follow.

Chapter 3 - The effects of frequency offset and timing offset are analyzed. A theoretical bound of for Signal to Interference Ratio (SIR) is derived. Moreover, a strategy of using null carriers to reduce the effect of ICI is discussed.

Chapter 4 - The acquisition algorithm is derived using the preamble of the OFDM packet. A maximum likelihood estimation function is first formulated. By differentiating the estimation function with respect to the channel coefficients and setting it to zero, the channel estimator is obtained. Using the orthogonality of the OFDM time samples, the timing and frequency offset

are extracted from the channel estimator. Analytical and Simulation results concludes the chapter.

Chapter 5 - The tracking algorithm is derived using the pilot tones in the data carrying part of the OFDM packet. Similar to the acquisition algorithm, a maximum likelihood estimation function is first formulated. The channel estimates, timing and frequency offset estimates are subsequently derived. Analytical and Simulation results concludes the chapter.

Chapter 6 - Concludes the findings in this thesis.

Chapter 2

Signal Model

In this chapter, we first describe the details of the OFDM system that will be considered for the joint channel estimation and synchronization (both timing and frequency). We first introduce the notation used. Then we described the OFDM packet used in IEEE 802.11a Wireless LAN standard. Finally we discuss the generation of the OFDM signal samples for transmission and the impairments to this signal due to channel effects like multipath propagation, additive noise, frequency offset and timing offset.

2.1   Notations

Standard notations are used in the thesis. Bold lowercase letters denote vectors while bold uppercase letters denote matrices. The real and imaginary parts are denoted as $\Re\{\cdot\}$ and $\Im\{\cdot\}$ while $diag(\mathbf{x})$ stands for a diagonal matrix

with $\mathbf{x}$ on its main diagonal. Other notations are as follows: $(\cdot)^t$ denotes transpose, $(\cdot)^*$ denotes complex conjugate, $(\cdot)^H$ denotes matrix Hermitian and $\hat{(\cdot)}$ denotes estimate of $(\cdot)$.

2.2 OFDM Packet

In the recently adopted IEEE 802.11 WLAN standard [12], each data packet consists of a preamble and a data carrying part as shown in fig. 2.1. The preamble consists of 10 "short" identical known OFDM symbols of length $N_s = 16$, $t_1, t_2, \ldots, t_{10}$, concatenated with 2 "long" identical and known OFDM symbols of length $N_l = 64$, T_1, T_2 that are used for carrier offset correction, channel estimation and synchronization. The data carrying part consists of a variable number of OFDM symbols of length $N_d = 64$ with N_o null carriers inserted at equal distance. Each OFDM symbol contains $N_d - N_o - N_P$ useful information symbols plus N_p pilot symbols, which are typically used for updating the channel estimates.
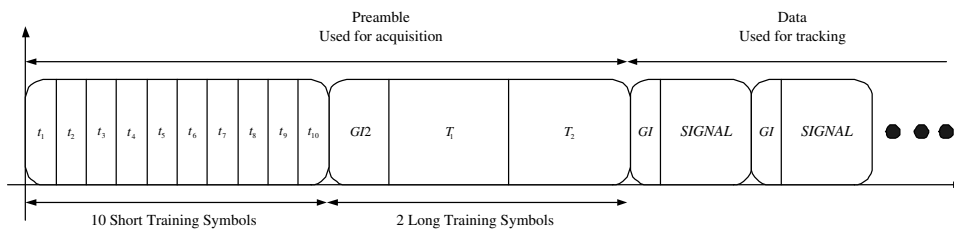
Figure 2.1: The structure of an OFDM packet

2.3 Signal Model

An OFDM symbol of length N is created by applying an inverse Fast Fourier Transform (IFFT) operator to N data symbols taken from a finite constellation, $\mathcal{A}$, such as BPSK, QPSK or QAM. Furthermore, each OFDM symbol is preceded by a cyclic prefix (CP) of length L that is an exact replica of the L last samples of the OFDM symbol. The block diagram of our OFDM system is shown in fig. 2.2.

Let Y_n and P_n denote the data and pilot symbol respectively taken from $\mathcal{A}$. The resulting N point time domain signal of variance σ_s^2 for the data carrying part are given by

$$
\begin{aligned}
s(k) =& m(k) + p(k) \\
=& \frac{1}{\sqrt{N}} \sum_{n=0}^{N_d-1} X_n e^{\frac{j2\pi nk}{N}}
\end{aligned}
\tag{2.1}
$$
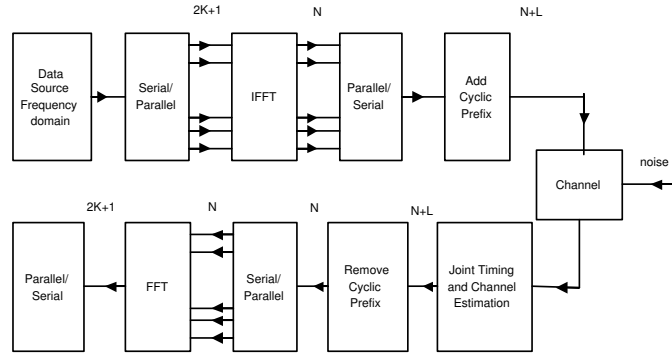
Figure 2.2: The baseband equivalent OFDM systems for our algorithm

where

$$X_n = \begin{cases} Y_n & n \in \{0, 1, \ldots, N-1\} \cap \overline{\Upsilon} \\ P_n & n \in \Upsilon \end{cases} \tag{2.2}$$

$$m(k) = \frac{1}{\sqrt{N}} \sum_{n \in \{0,1,\ldots,N-1\} \cap \overline{\Upsilon}} Y_n e^{\frac{j2\pi nk}{N}} \tag{2.3}$$

with mean zero and variance of $\sigma_m^2 = \left(\frac{N-N_p}{N}\right)\sigma_s^2$ denotes the output of the IFFT operator of the $N - N_p$ information carrying data subcarriers and

$$p(k) = \frac{1}{\sqrt{N}} \sum_{n \in \Upsilon} P_n e^{\frac{j2\pi nk}{N}} \tag{2.4}$$

denotes the output of IFFT operator of the N_p pilot subcarriers. Υ denotes the set of indices of the N_p pilot carriers.

For the preamble part, which is identical and constant for every OFDM packets, the resulting N point time domain signal of variance σ_s^2 is given by $s(k) = p(k)$.

2.4 Fading Channels

The classical way to model the transmission channel in a communications system is to use the additive white Gaussian noise (AWGH) channel, with statistically independent Gaussian noise samples corrupting data samples free of intersymbol interference (ISI). The AWGN channel is the usual starting point for understanding the basic performance of detectors. However, to

model practical mobile communications systems, time-varying and fading channels have to be considered. The following sub-sections describes the various types and characteristics of different fading channels.

2.4.1 Large-scale vs Small-scale fading

There are two types of fading effects that characterize mobile communications: large-scale fading and small-scale fading.

Large scale fading represents the average signal power attenuation or path loss due to motion over large areas. Such phenomenon is affected by prominent terrain contours such as hills, forests, high-rise buildings and so on between the transmitter and the receiver. The receiver is often represented as being shadowed by such prominence. The statistics of large-scale fading provide a way of computing an estimate of path loss as a function of distance. This is described in terms of a mean path loss and a log-normally distributed variation about the mean.

Small-scale fading refers to the rapid fluctuation of the amplitude of a radio signal over a short period of time or travel distance, so that the large-scale path loss effects may be neglected. Such fading is caused by interference between two or more versions of the transmitted signal which arrive at the receiver at slightly different times. These waves will combine at the receiver to give a resultant signal which can vary widely in amplitude and phase, depending on the distribution of the intensity and relative propagation time of the waves and the bandwidth of the transmitted signal.

In this thesis, only small scale fading will be considered, with the assumption that the communications between the mobile users and the base station occur within a relatively small area only. Thus no large-scale path loss has to be taken into account.

2.4.2 Rayleigh vs Rician Fading

For a mobile communications system used in the urban area, there is usually no line-of-sight (LOS) transmission between the mobile antennas and the base station due to the numerous high-rise buildings in the surroundings. Instead the mobile users communicate with the base station through a large number of multiple reflective paths. As a result, the envelope of the received signal is statistically described by a Rayleigh distribution. Such fading is called Rayleigh fading. The Rayleigh distribution has a probability density function (pdf) given by

$$p(r) = \frac{r}{\sigma^2} exp(-\frac{r^2}{2\sigma^2}), \tag{2.5}$$

where r is the envelope of the received signal and σ^2 is the time-average power of the received signal.

When there is a dominant non-fading signal component present, such as LOS propagation path, the small-scale fading envelope distribution is Rician. Thus the fading is called Rician fading. In such a situation, random multipath components arriving at different angles are superimposed on a dominant signal. At the output of an envelope detector, this has the effect of adding

a dc component to the random multipath. As the dominant signal becomes weaker, the composite signal resembles a noise signal which has a Rayleigh envelope. Thus the Rician distribution degenerates to a Rayleigh distribution when the dominant component fades away. The Rician pdf is given by

$$p(r) = \frac{r}{\sigma^2} exp(-\frac{r^2 + A^2}{2\sigma^2}) I_o(\frac{Ar}{\sigma^2}),\qquad(2.6)$$

where A is the peak amplitude of the dominant signal and $I_o(\cdot)$ is the modified Bessel function of the first kind and zero-order.

Compared with the Rician fading, the Rayleigh fading is more often used to model the mobile radio channels. As such in this thesis, emphasis will be put on the transmissions in Rayliegh fading channels.

2.4.3 Fast vs Slow Fading

Due to the relative motion between the mobile and the base station, each multipath wave experiences an apparent shift in frequency. The shift in received signal frequency due to motion is called the Doppler shift and is directly proportional to the speed and direction of motion of the mobile with respect to the direction of arrival of the received multipath wave. The maximal Doppler shift is called the Doppler spread. Doppler spread is a measure of the spectral broadening caused by the time rate of change of the mobile radio channel. It is a frequency parameter. Its corresponding time domain dual is called the coherence time. The coherence time of a channel is actually a statistical measure of the time duration over which the channel

impulse response is essentially invariant, and quantifies the similarity of the channel response at different times.

Both Doppler spread and coherence time describe the time varying nature of the communications channel in a small scale region. In fact, the doppler spread is inversely proportional to the coherence time. When the doppler spread is greater than the baseband signal bandwidth, or the coherence time is less than the symbol duration, the channel is said to be a fast fading channel. In a fast fading channel, the channel impulse response changes rapidly within the symbol duration. Thus the channel variations are faster than the baseband signal variations. Mathematically, the fast-fading channel impulse response within a symbol interval can be represented by a time varying wide-sense stationary uncorrelated scattering (WSSUS) model as

$$
\begin{aligned}
h(\tau, t) &= \sum_{l=0}^{N_m-1} f_l(t)\delta(\tau - \tau_l) \\
&= \sum_{l=0}^{N_m-1} \alpha_l(t)e^{j\phi_l(t)}\delta(\tau - \tau_l)
\end{aligned}
\tag{2.7}
$$

where N_m is the number of received paths, τ_l is the associated time delay, $f_l(t)$ represents the complex-valued time-varying channel coefficients of the lth path, $\alpha_l(t)$ is the Rayleigh distributed attenuation factor received on the lth path and $\phi_l(t)$ is the channel phase uniformly distributed over $[0, 2\pi]$.

On the other hand, when the doppler spread is much lower than the signal bandwidth, or the coherence time is much greater than the symbol duration, the channel is known as a slow fading one. In a slow fading chan-

nel, the channel impulse response changes at a rate much slower than the baseband signal. Hence the channel may be assumed to be static over one or several symbol intervals. The mathematical expression for the slow-fading channel impulse response within a symbol interval is

$$
\begin{aligned}
h(\tau, t) &= \sum_{l=0}^{N_m-1} f_l \delta(\tau - \tau_l) \\
&= \sum_{l=0}^{N_m-1} \alpha_l e^{j\phi_l} \delta(\tau - \tau_l).
\end{aligned}
\tag{2.8}
$$

A comparison between (2.7) and (2.8) shows that the channel coefficient f_l, channel gain α_l and the channel phase ϕ_l are no longer time-varying but constant within the symbol duration when the transmission channel is slow-fading.

In this thesis, slow fading channel is considered.

2.4.4   Flat vs Frequency Selective Fading

While the fast or slow fading describes the time variant nature of the communications channel, the flat or frequency selective fading characterizes the time spreading of the signal. To determine whether a channel is flat or frequency selective fading, the term "delay spread" has to be defined first. The delay spread is defined as the time between the first and last received component if a single transmitted signal during which the multipath signal power falls to some threshold level below that of the strongest component. The threshold level might be chosen at 10 or 20 dB below the level of the strongest

component. Analogous to delay spread in the time domain, coherence band-width is used to characterize the channel in the frequency domain. The delay spread and the coherence bandwidth are inversely proportional to each other although their exact relationship is a function of the multipath structure.

A signal undergoes flat fading if the symbol duration is much greater than the delay spread; or in the frequency domain, the signal bandwidth is much smaller than the coherence bandwidth. In such a case, the mobile radio channel has a constant gain and linear phase response over a bandwidth which is greater than the bandwidth of the transmitted signal. The multipath structure channel is such that the spectral characteristics of the transmitted signal are preserved at the receiver. However, the strength of the received signal changes with time, due to fluctuations in the gain of the channel caused by multipath. Flat fading channels are also known as narrowband channels since the bandwidth of the applied signal is narrow as compared to the coherence bandwidth.

On the contrary, if the symbol duration is smaller than the delay spread, or the signal bandwidth is greater than the coherence bandwidth, the channel is a frequency selective one. A frequency selective fading channel possesses a constant gain and linear phase over a bandwidth that is smaller than the bandwidth of the transmitted signal. Hence the received signal includes multiple versions of the transmitted waveform which are attenuated and de-layed in time, and thus the received signal is distorted. Frequency selective channels are also known as wideband channels since the signal bandwidth is wider than the bandwidth of the channel impulse response. As time varies,

the channel varies in gain and phase across the spectrum of the transmitted signal, thus resulting in time varying distortion in the received signal.

In this thesis, we developed joint channel estimation and synchronization algorithm for an OFDM system in a slow frequency selective fading environment.

2.5   Received Signal

Following the discussion of the communications channel in previous section, the effect of the propagation channel can be described by a finite impulse response (FIR) filter with an effective length of $N_m \leq L$, the received complex baseband signal can be written as

$$r(k) = \sum_{l=0}^{N_m-1} h_l s(k-l-\theta) e^{\frac{j2\pi\epsilon k}{N}} + n(k) \tag{2.9}$$

or in matrix form

$$\mathbf{r}(k) = \Phi \mathbf{S}(k)\mathbf{h} + \mathbf{n}(k) \tag{2.10}$$

$$\mathbf{r}(k) = [r(k), r(k+1), \ldots, r(k+N+L-1)]^t \tag{2.11}$$

$$\Phi = diag(e^{\frac{j2\pi\epsilon k}{N}}, e^{\frac{j2\pi\epsilon(k+1)}{N}}, \ldots, e^{\frac{j2\pi\epsilon(k+N+L-1)}{N}}) \tag{2.12}$$

$$\mathbf{S}(k) = [\mathbf{s}(k-\theta), \mathbf{s}(k-\theta-1), \ldots, \mathbf{s}(k-\theta-N_m+1)] \tag{2.13}$$

$$\mathbf{s}(k) = [s(k), s(k+1), \ldots, s(k+N+L-1)]^t \tag{2.14}$$

$$\mathbf{h} = [h_0, h_1, \ldots, h_{N_m-1}]^t \tag{2.15}$$

$$\mathbf{n}(k) = [n(k), n(k+1), \ldots, n(k+N+L-1)]^t \tag{2.16}$$

where $\{h_l\}$ denotes the slowly time-varying discrete time complex channel impulse response with $\sum_{l=0}^{N_m-1} E[|h_l|^2] = 1$. $\{n(k)\}$ is the time domain complex additive white Gaussian noise (AWGN) with variance σ_n^2, θ is the arrival time of the first multipath component and ϵ is the frequency offset which is defined as the difference in the transmitter and receiver oscillators as a fraction of the intercarriers spacing ($\frac{1}{N}$ in normalized frequency).

Chapter 3

Effect of Timing and Frequency Offset

In Chapter 1, we mentioned that the performance of OFDM system is very sensitive to time and frequency synchronization errors. In this chapter, we examine the effects of timing and carrier frequency offset on the system performance quantitatively. We will start with the effect of frequency offset.

3.1   Effect of Frequency Offset

In this section, we examine the effect of a frequency offset to an OFDM system. We will assume perfect timing synchronization. Thus, (2.9) becomes

$$
\begin{aligned}
r(k) &= \sum_{l=0}^{N_m-1} h_l s(k-l) e^{\frac{j2\pi\epsilon k}{N}} + n(k) \\
&= \sum_{l=0}^{N_m-1} h_l \frac{1}{\sqrt{N}} \sum_{m=0}^{N-1} X_m e^{\frac{j2\pi(k-l)m}{N}} e^{\frac{j2\pi\epsilon k}{N}} + n(k) \\
&= \frac{1}{\sqrt{N}} \sum_{m=0}^{N-1} X_m e^{\frac{j2\pi(m+\epsilon)k}{N}} \sum_{l=0}^{N_m-1} h_l e^{\frac{j2\pi l m}{N}} + n(k) \\
&= \frac{1}{\sqrt{N}} \sum_{m=0}^{N-1} X_m H_m e^{\frac{j2\pi(m+\epsilon)k}{N}} + n(k)
\end{aligned}
\tag{3.1}
$$

where H_m is the frequency transfer function of the channel at frequency of the mth carrier.

After FFT demodulation, we obtain the signal component as,

$$
\begin{aligned}
Y_n &= \frac{1}{\sqrt{N}} \sum_{k=0}^{N-1} r(k) e^{-\frac{j2\pi nk}{N}} \\
&= \frac{1}{N} \sum_{k=0}^{N-1} \sum_{m=0}^{N-1} X_m H_m e^{\frac{j2\pi(\epsilon+m-n)k}{N}} + \frac{1}{\sqrt{N}} \sum_{k=0}^{N-1} n(k) e^{-\frac{j2\pi nk}{N}} \\
&= \frac{1}{N} \sum_{m=0}^{N-1} X_m H_m dirc(\epsilon+m-n) + W_n
\end{aligned}
\tag{3.2}
$$

where

$$
dirc(x) = \sum_{k=0}^{N-1} e^{\frac{j2\pi x k}{N}}
$$

$$\begin{aligned}
&= \frac{e^{j2\pi x} - 1}{e^{\frac{j2\pi x}{N}} - 1} \\
&= \frac{e^{j\pi x} - e^{-j\pi x}}{e^{\frac{j\pi x}{N}}} - e^{\frac{j\pi x}{N}} e^{\frac{j\pi x(N-1)}{N}} \\
&= \left(\frac{\sin(\pi x)}{\sin\left(\frac{\pi x}{N}\right)} \right) e^{\frac{j\pi x(N-1)}{N}} \tag{3.3}
\end{aligned}$$

The modulated signal component in (3.2) can be expressed as a sum of the signal component, Z_n, an intercarrier interference (ICI) component, I_n and AWGN components as below

$$Y_n = Z_n + I_n + W_n \tag{3.4}$$

where

$$Z_n = X_n H_n \left(\frac{1}{N} dirc(\epsilon) \right) \tag{3.5}$$

$$I_n = \frac{1}{N} \sum_{m=0, m \neq n}^{N-1} X_m H_m dirc(\epsilon + m - n) \tag{3.6}$$

From (3.5), the presence of frequency offset reduces the useful signal amplitude. In addition, the loss of orthogonality between the OFDM carriers causes leakage from other subcarriers to subcarrier n, introducing ICI as given by (3.6).

Evaluating the statistical properties of Z_n and I_n,

$$E[|Z_n|^2] = E[|X_n H_n|^2] \left(\frac{1}{N^2} |dirc(\epsilon)|^2 \right) \tag{3.7}$$

$$E[|I_n|^2] = \frac{1}{N^2} \sum_{m=0,m\neq n}^{N-1} \sum_{k=0,k\neq n}^{N-1} E[X_m H_m X_k^* H_k^*]$$

$$dirc(\epsilon + m - n)dirc^*(\epsilon + k - n) \tag{3.8}$$

From Lemma 1 and assume the data symbols and the channel response are independent, i.e.

$$E[X_m H_m] = E[X_m H_m^*] = E[X_m^* H_m] = 0 \tag{3.9}$$

$$E[X_m X_k^* H_m H_k^*] = \sigma_h^2 \sigma_s^2 \delta_{m,k} \tag{3.10}$$

where

$$\sigma_h^2 = E[|H_m|^2] \tag{3.11}$$

Thus, we have

$$E[|Z_n|^2] = \frac{1}{N^2} \sigma_h^2 \sigma_s^2 |dirc(\epsilon)|^2 \tag{3.12}$$

$$E[|I_n|^2] = \frac{1}{N^2} \sigma_h^2 \sigma_s^2 \sum_{m=0,m\neq n}^{N-1} |dirc(\epsilon + m - n)|^2 \tag{3.13}$$

$$= \frac{1}{N^2} \sigma_h^2 \sigma_s^2 \sum_{m=0,m\neq n}^{N-1} \frac{\sin^2(\pi\epsilon)}{\sin^2(\frac{\pi(\epsilon+m-n)}{N})} \tag{3.14}$$

Define

$$ICI_{avg} = \frac{1}{N} \sum_{n=0}^{N-1} \left(\sum_{m=0,m\neq n}^{N-1} \frac{1}{N^2} |dirc(\epsilon + m - n)|^2 \right) \tag{3.15}$$

We examine the term in the summation in (3.15). Define

$$f(p) = \frac{1}{N^2} |dirc(\epsilon + p)|^2 \qquad (3.16)$$

This represents the ICI contribution by one subcarrier on another with p being the distance between them. We plot $f(p)$ for $N = 16$ for different ϵ in 3.1. The function is periodic with N and decreases sharply (super-linearly) as p increases towards $N/2$ before increasing sharply as p increases towards N.
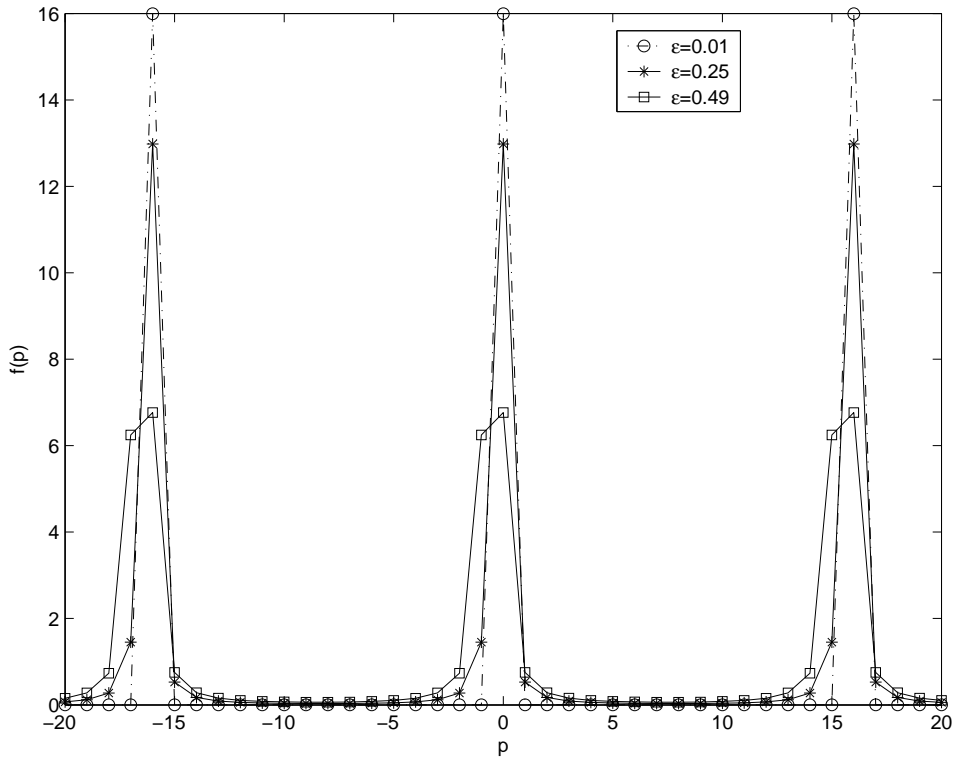

Figure 3.1: Plot of $f(p)$

3.1.1   Effect of Null Carriers

We have mentioned in Section 2.2 that the data carrying part consists of null carriers to loosen the frequency synchronization requirements. To visualize the benefit of inserting these null carriers, we shall provide below an analysis of the effect of null carriers on ICI arising from imperfect frequency offset compensation. The analysis can be used to lighten the frequency offset compensation requirement. This analysis is taken out from [13].

Firstly, we consider a system with N subcarrier and 2 activated subcarriers, labelled A and B, which are placed at carrier index k_1 and k_2. We assume that the carrier frequency offset is within half a subcarrier spacing but is equally probable to be positive or negative.

It is easy to see that the ICI power on A by B, depends on the circular distance between A and B as given by $\min(|k_1 - k_2|, N - |k_1 - k_2|)$. ICI_{Avg} is minimized when A and B are placed maximally apart at a distance of $N/2$ as shown in fig. 3.2.
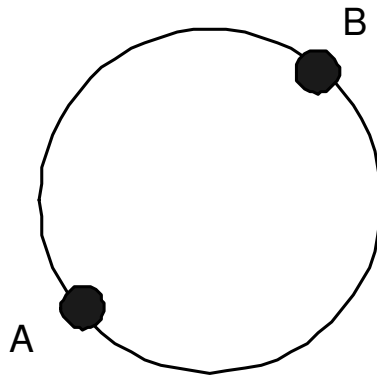

Figure 3.2: Illustration to show ICI_{Avg} is minimum when A and B is placed at equidistance apart

Next we consider the case where there are 3 activated carriers, A, B and C placed at equidistance d apart as shown in fig. 3.3. Since $f(d) - f(d+|\delta|) < f(d-|\delta|) - f(d)$, for $|\delta| < d$ and $d+|\delta| < N/2$, the penalty incurred in moving the subcarrier A towards B by $|\delta|$ is higher than the reduction in penalty as subcarrier being shifted away from C. Using this argument, and fixing the placement of C, shifting either A or B or both would result in the increment in ICI_{Avg}.
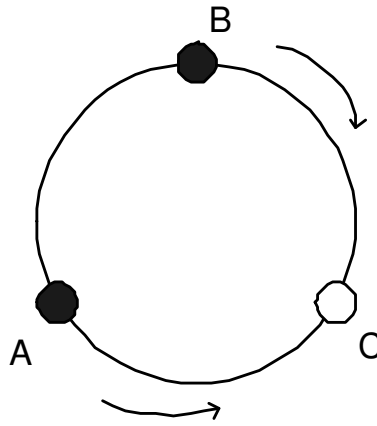
Figure 3.3: Illustration to show moving A and B towards C increases ICI of C (and vice versa) on B. This is larger than the reduction of ICI on A and B by each other

For example, shifting A and B towards C would increase the ICI power on C by A and B (and vice versa). This increment is larger than the decrement in the ICI power on A and B (and vice versa) as they are shifted away from each other. Hence, ICI_{Avg} is minimum when A, B and C are placed at equidistance apart as in the case of 2 subcarriers.

As shown in fig. 3.1, ICI contributed by a consecutive activated subcarrier is much higher than that at other positions. This suggests that ICI_{Avg} is maximum when all the activated subcarriers are equally spaced, if possible.

However, since the the subcarriers can only be placed at discrete positions, we argue that the following approach will minimize ICI_{avg}:

1. When the number of null subcarriers exceeds the number of activated subcarriers, the activated subcarriers should be distributed at equidistance apart.

2. When the number of activated subcarriers exceed the number of null subcarriers, the null subcarriers should be distributed at equidistance apart. This will minimize the number of consecutive activated subcarriers.

3.1.2   Theoretical Bound for Signal Interference Ratio

In this subsection, we derive the theoretical bound for signal interference ratio caused by frequency offset. Using the property that $\sin^2(\frac{\pi x}{N})$ is periodic with period N, the summation is shown in (3.14) is shown to be independent of n, as seen below.

$$
\frac{1}{N^2} \sum_{m=0, m\neq n}^{N-1} \frac{1}{\sin^2\left(\frac{\pi(\epsilon+m-n)}{N}\right)} = \frac{1}{N^2} \sum_{p=-n, \, p\neq 0}^{N-1-n} \frac{1}{\sin^2\left(\frac{\pi(\epsilon+p)}{N}\right)}
$$

$$
= \frac{1}{N^2} \sum_{p=1}^{N-1} \frac{1}{\sin^2\left(\frac{\pi(\epsilon+p)}{N}\right)} \tag{3.17}
$$

For our analysis, we restrict the frequency offset ϵ to be within ± 0.5 since exceeding this range, the correspondence between the demodulated sequence Y_n and the original sequence X_n for each n will not be distinguishable.

The summation in (3.17) is an even function with respect to ϵ and it has been numerically shown in [14] that the summation is monotonically increasing with $|\epsilon|$. In addition, its variation with N is negligible for $N \geq 256$ (usually less than 10^{-6}). Substituting $\epsilon = 0$ and $|\epsilon| = 0.5$, we obtain the following inequality,

$$0.3333|_{\epsilon=0} \leq \frac{1}{N^2} \sum_{p=1}^{N-1} \frac{1}{\sin^2(\frac{\pi(\epsilon+p)}{N})} \leq 0.5487|_{|\epsilon|=0.5} \qquad (3.18)$$

We define the average Signal to Interference Ratio, SIR_{Avg} as

$$SIR_{Avg} = \frac{1}{N} \sum_{n=0}^{N-1} \frac{E[|X_n|^2]}{E[|I_n|^2] + E[|W_n|^2]} \qquad (3.19)$$

Using the inequality (3.18),

$$
\begin{aligned}
SIR_{Avg} &\geq \frac{1}{N^2} \frac{\sigma_h^2 \sigma_s^2 |dirc(\epsilon)|^2}{0.5497\sigma_h^2 \sigma_s^2 \sin^2(\pi\epsilon) + N^2 \sigma_n^2} \\
&= \frac{1}{N^2} \frac{|dirc(\epsilon)|^2}{0.5497 \sin^2(\pi\epsilon) + \frac{N^2 \sigma_n^2}{\sigma_h^2 \sigma_s^2}} \\
&= \frac{1}{N^2} \frac{|dirc(\epsilon)|^2}{0.5497 \sin^2(\pi\epsilon) + SNR^{-1}}
\end{aligned}
\qquad (3.20)
$$

where the signal to noise ratio is defined as $SNR = \frac{N^2 \sigma_n^2}{\sigma_h^2 \sigma_s^2}$.

In fig. 3.4, we show the lower bound as given by (3.20) for an OFDM system with $N = 256$ subcarriers for different ϵ. It can be easily seen that the bound saturates at high SNR value. This is due to the fact that at high SNR value, SNR^{-1} in the denominator value of (3.20) tends to zero. Next

we show the degradation in SNR which is defined as

$$Degradation = SNR - SIR \qquad (3.21)$$

in fig. 3.5. It can be easily seen that the degradation increases linearly at high SNR value. From this perspective, the OFDM system should be operated at the lowest SNR value that yield the desired error rate. For example, a system operating at an SNR of 10dB will experience a degradation of less than 5dB for frequency offset of 10%. A system operating at 30dB will experience degradation of about 22dB. These values are higher bound as the degradation is calculated using the lower bound of (3.20).
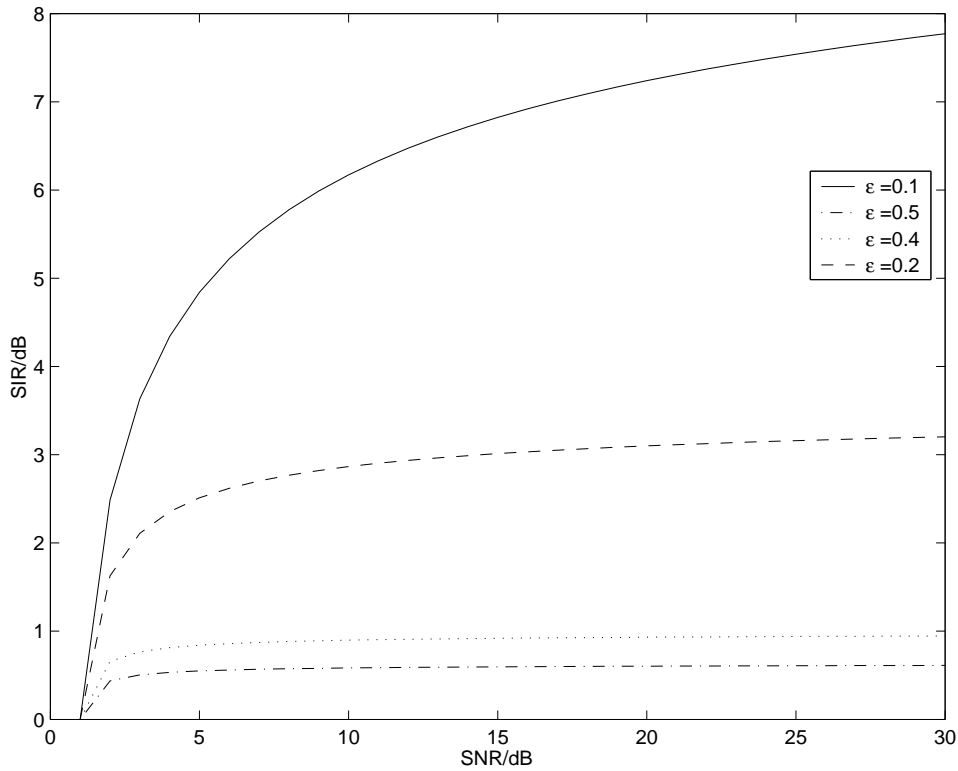
Figure 3.4: SIR vs SNR

Figure 3.5: Degradation in SNR
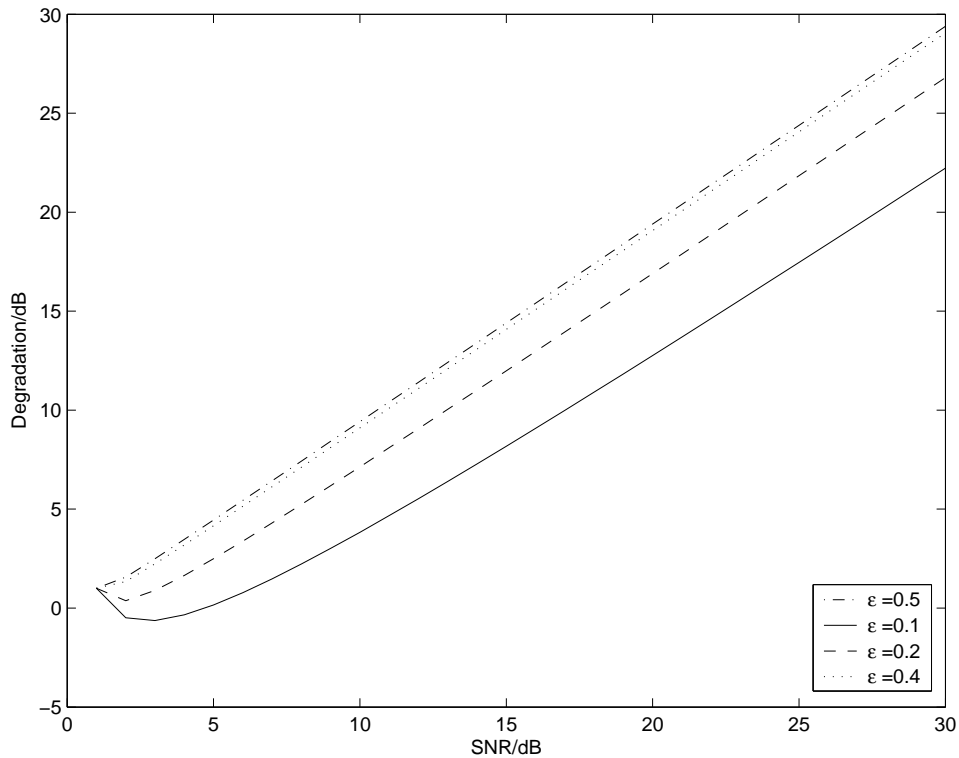
3.2 Effect of Timing Offset

In this section, we are concerned with the analysis of the effect of symbol timing errors and we make the following assumptions:

1. The OFDM systems considered are synchronized in terms of sampling clock frequency.

2. The carrier frequencies are perfectly synchronized.

3. There are 2 cases as depicted in fig. 3.6. We confined ourselves to the

case where the start position of the FFT window is within region A, i.e no ISI occurs.
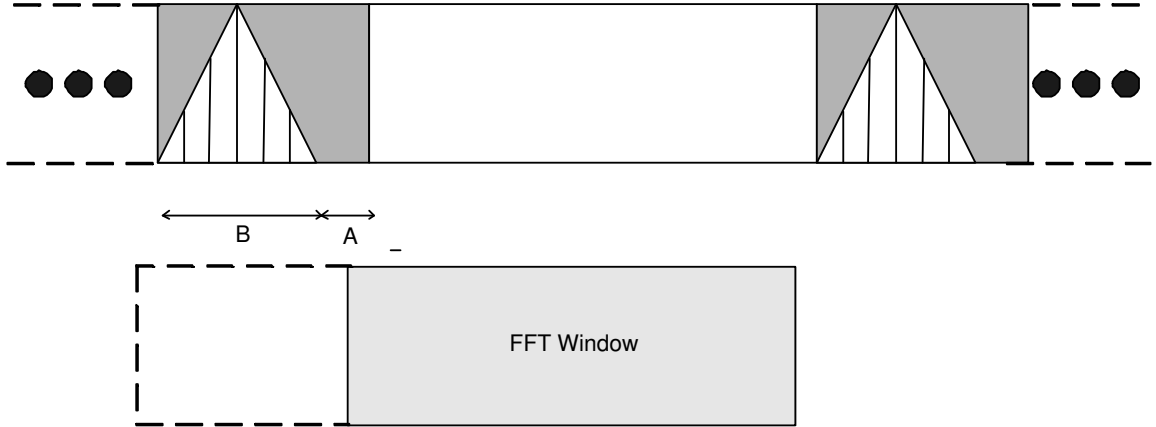
Figure 3.6: Frame synchronization region

With the above assumptions in mind, the signal received can be expressed in the form:

$$r(t) = \sum_{m=0}^{N-1} X_m e^{\frac{j2\pi m(t-\tau)}{T}} e^{j2\pi f_o t} H_m \tag{3.22}$$

Rearranging the terms,

$$r(t) = e^{j2\pi f_o t} \sum_{m=0}^{N-1} X_m e^{-\frac{j2\pi m\tau}{T}} e^{\frac{j2\pi mt}{T}} H_m \tag{3.23}$$

The received signal is typically down-converted to baseband, sampled and then applied to an FFT demodulator as a first step in the data detection process. When the number of carriers is relatively large, the function of the FFT block is nearly equivalent to a bank of N correlators. The output of

the nth correlator is equivalent to the nth FFT coefficient.

The output of the nth correlator is of the form:

$$X_n = \frac{1}{T} \int_0^T e^{-\frac{j2\pi nt}{T}} \sum_{m=0}^{N-1} X_m e^{\frac{j2\pi mt}{T}} e^{-\frac{j2\pi m\tau}{T}} H_m dt \qquad (3.24)$$

which can be rearranged as

$$X_n = \sum_{m=0}^{N-1} \frac{X_m H_m}{T} e^{-\frac{j2\pi m\tau}{T}} \int_0^T e^{\frac{j2\pi(m-n)t}{T}} dt \qquad (3.25)$$

The desired component of X_n (corresponding to the data symbol of the nth subcarrier) is

$$X_n|_{desired} = X_n H_n e^{-\frac{j2\pi n\tau}{T}} \qquad (3.26)$$

which is the nth symbol modified by the frequency response of the channel and rotated by an angle which depends on the frequency index n and on the relative delay. The interfering component of X_n is of the form

$$X_n|_{interference} = \sum_{m=0,\, m\neq n}^{N-1} \frac{X_m H_m}{T} e^{-\frac{j2\pi m\tau}{T}} \int_0^T e^{\frac{j2\pi(m-n)t}{T}} dt$$

$$= 0 \qquad (3.27)$$

The timing errors do not produce an additive interference term as it was with the frequency offset. It can be concluded that the timing error results in a rotation of the received symbols. The set of rotations experienced by all frequency tones makes up a random variable. These rotations are additional

and cannot be distinguished to any rotation caused by the channel gain coefficients, H_n. The aggregate rotation must be taken care of a frequency domain equalizer.

Chapter 4

Acquisition Algorithm

In this chapter, we derive the maximum-likelihood estimation function on which our acquisition algorithm is based. The acquisition algorithm is formulated using the two "long" training symbols in the preamble. An analytical study of the performance was given.

4.1 Property of OFDM Time Samples

In this section, we state the following property of transmitted OFDM time samples, $s(k)$, given in (2.1), which will be used throughout this chapter.

Lemma 1 *The transmitted OFDM time samples excluding cyclic prefix are independent identically distributed (i.i.d) Gaussian random variables provided the frequency domain data are i.i.d.*

Proof From (2.1), $s(k)$ is Gaussian by Central Limit Theorem. To prove independence of $s(k)$, we calculate

$$
\begin{aligned}
E\{s(a)s^*(b)\} &= \frac{1}{N}\sum_{n=0}^{N-1}\sum_{m=0}^{N-1} E\{X_n X_m^*\} e^{\frac{j2\pi(na-mb)}{N}} \\
&= \frac{1}{N}\sum_{n=0}^{N-1} E\{X_n X_n^*\} e^{\frac{j2\pi(a-b)n}{N}} \\
&= \frac{1}{N}E\{|X|^2\}\sum_{n=0}^{N-1} e^{\frac{j2\pi(a-b)n}{N}} \\
&= \begin{cases} \sigma_s^2 & \text{if } a=b \\ \sigma_s^2 & \text{if } b=a+N, a \in \text{cyclic prefix} \\ 0 & \text{elsewhere} \end{cases}
\end{aligned}
\tag{4.1}
$$

where we have used the well-known identity in signal processing, $\sum_{k=0}^{N-1} e^{\frac{j2\pi(a-b)n}{N}} = N$ for $a=b+cN$ and is zero otherwise as shown below

$$
\begin{aligned}
\sum_{n=0}^{N-1} e^{\frac{j2\pi(a-b)n}{N}} &= \frac{e^{j2\pi(a-b)}-1}{e^{\frac{j2\pi(a-b)}{N}}-1} \\
&= \frac{e^{j\pi(a-b)}\left(e^{j\pi(a-b)}-e^{-j\pi(a-b)}\right)}{e^{\frac{j\pi(a-b)}{N}}\left(e^{\frac{j\pi(a-b)}{N}}-e^{\frac{-j\pi(n-m)}{N}}\right)} \\
&= \frac{e^{j\pi(a-b)}sin\left((a-b)\pi\right)}{e^{\frac{j\pi(a-b)}{N}}sin\left(\frac{(a-b)\pi}{N}\right)} \\
&= \begin{cases} N & \text{if } a=b+cN \\ 0 & \text{elsewhere} \end{cases}
\end{aligned}
\tag{4.2}
$$

In (4.1), we proved that transmitted time domain OFDM samples excluding cyclic prefix are orthogonal to each other. Since the mean of the

samples is zero, $E[s(a)] = E[s(b)] = 0$, the OFDM samples are uncorrelated and hence independent to each other.

4.2 ML Algorithm for Acquisition

In this section, we deal with acquiring the estimates of the channel coefficients, h_i, the arrival time of the first multipath component, θ and the frequency offset, ϵ using the two "long" training symbols in preamble. Assume we transmit N_l consecutive samples of the two "long" training symbols in the preamble, $s(k)$ starting from $s(0)$ and observe $N_l + N_m$ consecutive samples of $r(k)$ starting from $r(\theta)$. We then define $\mathbf{p} \stackrel{\triangle}{=} [s(0), s(1), \ldots, s(N_l - 1)]^t$ as the $N_l \times 1$ vector of the transmitted samples and $\mathbf{r} \stackrel{\triangle}{=} [r(\theta), r(\theta+1), \ldots, r(\theta+N_l + N_m - 1)]^t$ as the $(N_l + N_m) \times 1$ vector of the observed samples. Notice that the received OFDM samples given in (2.9) conditioned on $\theta, \epsilon, \mathbf{h}, \mathbf{p}$, denoted as $\{r(k)|(\theta, \epsilon, \mathbf{h}, \mathbf{p})\}$ are i.i.d Gaussian with mean,

$$
\mu_k = \begin{cases}
\sum_{l=0}^{k-\theta} h_l s(k - \theta - l) e^{\frac{j2\pi\epsilon k}{N}} & \theta \le k \le \theta + N_m - 1 \\
\sum_{l=0}^{N_m-1} h_l s(k - \theta - l) e^{\frac{j2\pi\epsilon k}{N}} & \theta + N_m \le k \le \theta + N_l - 1 \\
\sum_{l=k-\theta-N_l}^{N_m-1} h_l s(k - \theta - l) e^{\frac{j2\pi\epsilon k}{N}} & \theta + N_l \le k \le \theta + N_l + N_m - 1
\end{cases}
$$

$$(4.3)$$

and variance, σ_n^2. Thus, the conditional pdf is given by

$$
f(\mathbf{r}|\theta, \epsilon, \mathbf{h}, \mathbf{p}) = \frac{1}{(\pi\sigma_n^2)^{N_l+N_m}} exp\Big(- \frac{\sum_{k=\theta}^{\theta+N_l+N_m-1} |r(k) - \mu_k|^2}{\sigma_n^2} \Big),
$$

while the log-likelihood function of $\mathbf{h}$, θ and ϵ is

$$\Lambda_a(\mathbf{h}, \theta, \epsilon) = -\sum_{k=\theta}^{\theta+N_l+N_m-1} |r(k) - \mu_k|^2$$

after dropping all the constants.

Although h_i is complex, our log-likelihood function is real and concave. Applying the complex gradient operator proposed in [15], our channel estimate will be the solution of

$$\nabla_{h_i}^c \Lambda_a = 0$$

where

$$\nabla_{h_i}^c = \frac{\partial}{\partial h_{i,R}} + j\frac{\partial}{\partial h_{i,I}}. \tag{4.4}$$

With that, we obtain

$$\begin{aligned}
\nabla_{h_i}^c \Lambda &= -\sum_{k=\theta}^{\theta+N_l+N_m-1} \nabla_{h_i}^c \left(|r(k) - \mu_k|^2 \right) \\
&= \sum_{k=\theta}^{\theta+N_l+N_m-1} \left(r(k) - \mu_k \right) \nabla_{h_i}^c \mu_k^* + \sum_{k=\theta}^{\theta+N_l+N_m-1} \left(r^*(k) - \mu_k^* \right) \nabla_{h_i}^c \mu_k
\end{aligned}$$

$$\tag{4.5}$$

Applying the definition of (4.4),

$$\nabla^c_{h_i} h_i = \frac{\partial h_i}{\partial h_{i,R}} + j\frac{\partial h_i}{\partial h_{i,I}}$$

$$= 1 + j(j)$$

$$= 0, \tag{4.6}$$

while

$$\nabla^c_{h_i} h_i^* = \frac{\partial h_i^*}{\partial h_{i,R}} + j\frac{\partial h_i^*}{\partial h_{i,I}}$$

$$= 1 + j(-j)$$

$$= 2. \tag{4.7}$$

Applying (4.6) and (5.1) to (4.5), the second term is zero while expanding the first term according to (5.1), we obtain

$$\nabla^c_{h_i}\Lambda = \sum_{k=\theta}^{\theta+N_m-1} \left(r(k) - \sum_{l=0}^{k-\theta} h_l s(k-\theta-l)e^{\frac{j2\pi\epsilon k}{N}}\right) \sum_{l'=0}^{k-\theta} \nabla^c_{h_i} h_{l'}^* s^*(k-\theta-l')e^{-\frac{j2\pi\epsilon k}{N}}$$

$$+ \sum_{k=\theta+N_m}^{\theta+N_l-1} \left(r(k) - \sum_{l=0}^{N_m-1} h_l s(k-\theta-l)e^{\frac{j2\pi\epsilon k}{N}}\right) \sum_{l'=0}^{N_m-1} \nabla^c_{h_i} h_{l'}^* s^*(k-\theta-l')e^{-\frac{j2\pi\epsilon k}{N}}$$

$$+ \sum_{k=\theta+N_l}^{\theta+N_l+N_m-1} \left(r(k) - \sum_{l=k-\theta-N_l}^{N_m-1} h_l s(k-\theta-l)e^{\frac{j2\pi\epsilon k}{N}}\right) \sum_{l'=k-\theta-N_l}^{N_m-1} \nabla^c_{h_i} h_{l'}^* s^*(k-\theta-l')e^{-\frac{j2\pi\epsilon k}{N}}.$$

Substituting (4.7), and varying the index of k in the first summation to make

sure the index l' in the third summation will contain the value i,

$$
\begin{aligned}
\nabla_{h_i}^c = 2 & \sum_{k=\theta+i}^{\theta+N_m-1} \left(r(k) - \sum_{l=0}^{k-\theta} h_l s(k-\theta-l) e^{\frac{j2\pi\epsilon k}{N}} \right) s^*(k-\theta-i) e^{-\frac{j2\pi\epsilon k}{N}} \\
+ 2 & \sum_{k=\theta+N_m}^{\theta+N_l-1} \left(r(k) - \sum_{l=0}^{N_m-1} h_l s(k-\theta-l) e^{\frac{j2\pi\epsilon k}{N}} \right) s^*(k-\theta-i) e^{-\frac{j2\pi\epsilon k}{N}} \\
+ 2 & \sum_{k=\theta+N_l}^{\theta+N_l+i-1} \left(r(k) - \sum_{l=k-\theta-N_l}^{N_m-1} h_l s(k-\theta-l) e^{\frac{j2\pi\epsilon k}{N}} \right) s^*(k-\theta-i) e^{-\frac{j2\pi\epsilon k}{N}} \\
= 2 & \sum_{k=\theta+i}^{\theta+N_l+i-1} r(k) s^*(k-\theta-i) e^{\frac{-j2\pi\epsilon k}{N}} \\
- 2 & \sum_{k=\theta+i}^{\theta+N_m-1} \sum_{l=0}^{k-\theta} h_l s(k-\theta-l) s^*(k-\theta-i) \\
- 2 & \sum_{k=\theta+N_m}^{\theta+N_l-1} \sum_{l=0}^{N_m-1} h_l s(k-\theta-l) s^*(k-\theta-i) \\
- 2 & \sum_{k=\theta+N_l}^{\theta+N_l+i-1} \sum_{l=k-\theta-N_l}^{N_m-1} h_l s(k-\theta-l) s^*(k-\theta-i)
\end{aligned}
\tag{4.8}
$$

From Lemma I, we have $\sum_{k=a}^{b-1} s(k-\theta-l) s^*(k-\theta-i) = (b-a)\sigma_s^2 \delta_{i,l}$ and applying this to the right hand side of (4.8) and setting it to zero, we obtain

$$
\hat{h}_i = \frac{1}{N_l \sigma_s^2} \sum_{k=\theta+i}^{\theta+N_l+i-1} r(k) s^*(k-\theta-i) e^{-\frac{j2\pi\epsilon k}{N}}
\tag{4.9}
$$

for $i = 0, 1, \ldots, N_m - 1$.

(4.9) shows that our channel estimator is a simple correlator. To obtain the channel estimates, h_i, we correlate N_l received samples with the phase

shifted pilot symbols starting at the time instant $\theta + i$. Furthermore, note that we arrived at (4.9) by conditioning on θ and ϵ, i.e. we implicitly assumed that θ and ϵ are known a priori or the receiver is perfectly symbol and frequency synchronized. However, before perfect symbol and frequency synchronization, θ and ϵ are unknown and we only have their estimates, $\hat{\theta}$ and $\hat{\epsilon}$. Thus, (4.9) should be

$$\hat{h}_i = \frac{1}{N_l \sigma_s^2} \sum_{k=\hat{\theta}+i}^{\hat{\theta}+N_l+i-1} r(k)s^*(k - \hat{\theta} - i)e^{-\frac{j2\pi\hat{\epsilon}k}{N}}. \qquad (4.10)$$

Substituting (2.9) into (4.10), we obtain

$$\hat{h}_i = \frac{1}{N_l \sigma_s^2} \sum_{k=\hat{\theta}+i}^{\hat{\theta}+N_l+i-1} \sum_{l=0}^{N_m-1} h_l s(k - \theta - l)s^*(k - \hat{\theta} - i)e^{\frac{j2\pi(\epsilon-\hat{\epsilon})k}{N}}$$

$$+ \frac{1}{N_l \sigma_s^2} \sum_{k=\hat{\theta}+i}^{\hat{\theta}+N_l+i-1} n(k)s^*(k - \hat{\theta} - i)e^{-\frac{j2\pi\hat{\epsilon}k}{N}}. \qquad (4.11)$$

Due to the orthogonality of OFDM time samples as shown in Lemma 1, the first term in (4.11) will be nonzero only for $\hat{\theta} = \theta - i + l$. Furthermore, (4.11) will reach maximum only when $\hat{\epsilon} = \epsilon$. For other values of $\hat{\epsilon}$, the first term in (4.11) will not add coherently. Thus, we are able to extract the timing and frequency offset from our channel estimator by varying $\hat{\theta}$ and $\hat{\epsilon}$ over all the possible values, regardless of i, and search for the index that maximizes $|\sum_{k=\hat{\theta}}^{\hat{\theta}+N_l-1} r(k)s^*(k - \hat{\theta})e^{-\frac{j2\pi\hat{\epsilon}k}{N}}|$.

4.3   The Acquisition Algorithm

The acquisition algorithm is summarized as below:

1. Form a length N_l received vector, $\mathbf{r}(a) = [r(a), \ldots, r(a + N_l - 1)]^t$

2. Compute $\gamma(a, \hat{\epsilon}) = \frac{1}{N_l \sigma_s^2} \hat{\Phi}^H \mathbf{p}^H \mathbf{r}(a)$, where $\mathbf{p}$ is the pilot vector containing one of the two "long" identical training symbol in the preamble as defined in Section 4.2 and $\hat{\Phi} = diag(e^{\frac{j2\pi\hat{\epsilon}a}{N}}, e^{\frac{j2\pi\hat{\epsilon}(a+1)}{N}}, \ldots, e^{\frac{j2\pi\hat{\epsilon}(a+N_l-1)}{N}})$. This when expanded will be (4.10).

3. $\beta(a, \hat{\epsilon}) = \sum_{k=a}^{a+N_m-1} |\gamma(k, \hat{\epsilon})|$.

4. $\{\hat{\theta}, \hat{\epsilon}\} = \arg\{max\{\beta(a, \hat{\epsilon})\}\}$.

5. $\hat{h_0}, \hat{h_1}, \ldots, \hat{h}_{N_m-1} = \gamma(\hat{\theta}, \hat{\epsilon}), \gamma(\hat{\theta} + 1, \hat{\epsilon}), \ldots, \gamma(\hat{\theta} + N_m - 1, \hat{\epsilon})$.

Firstly, we correlate our received samples with the phase shifted training symbol in the preamble. We vary the value of $\hat{\epsilon}$ in a fix step size from -1 to 1 for each i. Then, in step 3), we coherently combine the contribution of the multipath such that we are always able to synchronize to the first arriving path even though it is not the strongest path. In step 4, we search for the arrival time of the first multipath component, $\hat{\theta}$ and the frequency offset, $\hat{\epsilon}$. Finally, we estimate the channel coefficients accordingly.

4.4 Performance Analysis

In this section, we analytically examine the performance of our channel estimation and symbol synchronization algorithm for the acquisition stage.

4.4.1 Analytical Expression for Probability of Correct Synchronization

When demodulating the received data in a multipath fading environment, it is crucial for the receiver to synchronize to the first arrival path such that when the cyclic prefix is discarded, ISI can be removed during OFDM demodulation. Thus, we measure our symbol synchronization algorithm in terms of probability of synchronizing to the first arrival path. With this performance measure, we have

$$
\begin{aligned}
P_{c|\hat{\epsilon}=\epsilon} =& P(\hat{\theta} = \theta) \\
=& P\big(\beta(\theta, \epsilon) \geq \beta(1, \epsilon), \beta(2, \epsilon), \ldots, \beta(M, \epsilon)\big) \\
=& \int_0^\infty P\big(\beta(1, \epsilon) \leq \beta(\theta, \epsilon), \ldots, \beta(M, \epsilon) \leq \beta(\theta, \epsilon) | \beta(\theta, \epsilon) = x\big) f_{\beta(\theta, \epsilon)}(x) dx.
\end{aligned}
$$

(4.12)

From the joint pdf of β, (A.11), derived in Appendix A, we note that β are not independent. Thus, it is unfeasible to evaluate (4.12) as it requires a M dimension integration. However, we are able to calculate the probability of synchronizing to any path using the pdf of $|\gamma|$, (A.10), derived in Appendix A

as below

$$P'_{c|\hat{\epsilon}=\epsilon} = P'(\hat{\theta} = \theta) + P'(\hat{\theta} = \theta + 1) + \ldots + P'(\hat{\theta} = \theta + N_m - 1) \qquad (4.13)$$

where

$$
\begin{aligned}
P'(\hat{\theta} = \theta) &= P\big(z_\theta \geq z_1, z_2, \ldots, z_M\big) \\
&= \int_0^\infty P(z_1 \leq z_\theta, z_2 \leq z_\theta, \ldots, z_M \leq z_\theta | z_\theta = x) f_{z_\theta}(x) dx.
\end{aligned}
$$

4.4.2 Mean and Variance of Channel Estimation Error

We conduct a first order performance analysis on our proposed channel estimator by evaluating the mean and variance of the estimation error.

Lemma 2 *The estimator is unbiased, consistent and efficient. In addition, the MSE of the channel estimate, $\hat{h}_i$ is*

$$E\{|h_i - \hat{h}_i|^2\} = \frac{1}{N_l} \frac{\sigma_n^2}{\sigma_s^2}$$

which is the same as the result in [16].

Proof

$$E\{\hat{h}_i\} = \frac{1}{N_l \sigma_s^2} \sum_{k=\theta+i}^{\theta+N_l+i-1} E\{r(k)\} s^*(k - \theta - i) e^{-\frac{j2\pi\epsilon k}{N}}$$

$$= \frac{1}{N_l \sigma_s^2} \sum_{k=\theta+i}^{\theta+N_l+i-1} \sum_{l=0}^{N_m-1} h_l s(k - \theta - l) s^*(k - \theta - i) = h_i$$

Thus, the channel estimator is unbiased.

$$E\{|h_i - \hat{h}_i|^2\} = E\{|\hat{h}_i|^2\} - |h_i|^2 \tag{4.14}$$

To calculate the first term of the RHS of (4.14), we note that

$$\begin{aligned}
E\{|\hat{h}_i|^2\} =& \frac{1}{N_l^2 \sigma_s^4} \mathbf{p}^H \Phi^H E\{\mathbf{r}(\theta + i)\mathbf{r}^H(\theta + i)\}\Phi\mathbf{p} \\
=& \frac{1}{N_l^2 \sigma_s^4} \mathbf{p}^H \Phi^H E\{[\Phi\mathbf{S}(\theta + i)\mathbf{h} + \mathbf{n}(\theta + i)][\mathbf{h}^H \mathbf{S}^H(\theta + i)\Phi^H + \mathbf{n}(\theta + i)]\}\Phi\mathbf{p} \\
=& \frac{1}{N_l^2 \sigma_s^4} \mathbf{p}^H \mathbf{S}(\theta + i)\mathbf{h}\mathbf{h}^H \mathbf{S}^H(\theta + i)\mathbf{p} + \frac{1}{N_l^2 \sigma_s^4} \mathbf{p}^H \Phi^H E\{\mathbf{n}(\theta + i)\mathbf{n}^H(\theta + i)\}\Phi\mathbf{p} \\
=& |h_i|^2 + \frac{1}{N_l}\frac{\sigma_n^2}{\sigma_s^2}.
\end{aligned}$$

Thus, the MSE of our estimator is

$$E\{|h_i - \hat{h}_i|^2\} = \frac{1}{N_l}\frac{\sigma_n^2}{\sigma_s^2}.$$

Since the MSE approaches zero when the number of observation samples approaches infinity, the channel estimator is consistent.

4.5   Simulation Results and Discussions

In this section, the performance of the acquisition algorithm is evaluated using computer simulation under simple AWGN channel and multipath Rayleigh fading channel. Particularly, mse value, pdf and probability of correct synchronization are used to evaluate the performance.

4.5.1   Performance in AWGN Channel

An AWGN channel can be modelled using (2.9) by letting $N_m = 1$ and $h_0 = 1$. Thus the acquisition algorithm derived can be modified accordingly as below to estimate θ and ϵ:

1. Form a length N_l received vector, $\mathbf{r}(a) = [r(a), \ldots, r(a + N_l - 1)]^t$

2. Compute $\gamma(a, \hat{\epsilon}) = \frac{1}{N_l \sigma_{\tilde{s}}^2} \hat{\Phi}^H \mathbf{p}^H \mathbf{r}(a)$, where $\mathbf{p}$ is the pilot vector containing one of the two "long" identical training symbol in the preamble as defined in Section 4.2 and $\hat{\Phi} = diag(e^{\frac{j2\pi\hat{\epsilon}a}{N}}, e^{\frac{j2\pi\hat{\epsilon}(a+1)}{N}}, \ldots, e^{\frac{j2\pi\hat{\epsilon}(a+N_l-1)}{N}})$.

3. $\{\hat{\theta}, \hat{\epsilon}\} = \arg\{max\{gamma(a, \hat{\epsilon})\}\}$.

To demonstrate the performance of our synchronization algorithm, we compare the performance of our acquisition algorithm to that of Schmidl and Cox [1] which has been used to obtain an initial timing estimate in [17]. The algorithm in [1] declares symbol synchronization at the position a, for which

the following function is maximized:

$$M(a) = \frac{|P(a)|^2}{\big(R(a)\big)^2} = \frac{|\sum_{k=0}^{N_l-1} r^*(a+k)r(a+k+N_l)|^2}{\big(\sum_{k=0}^{N_l-1} |r(a+k+N_l)|^2\big)^2} \qquad (4.15)$$
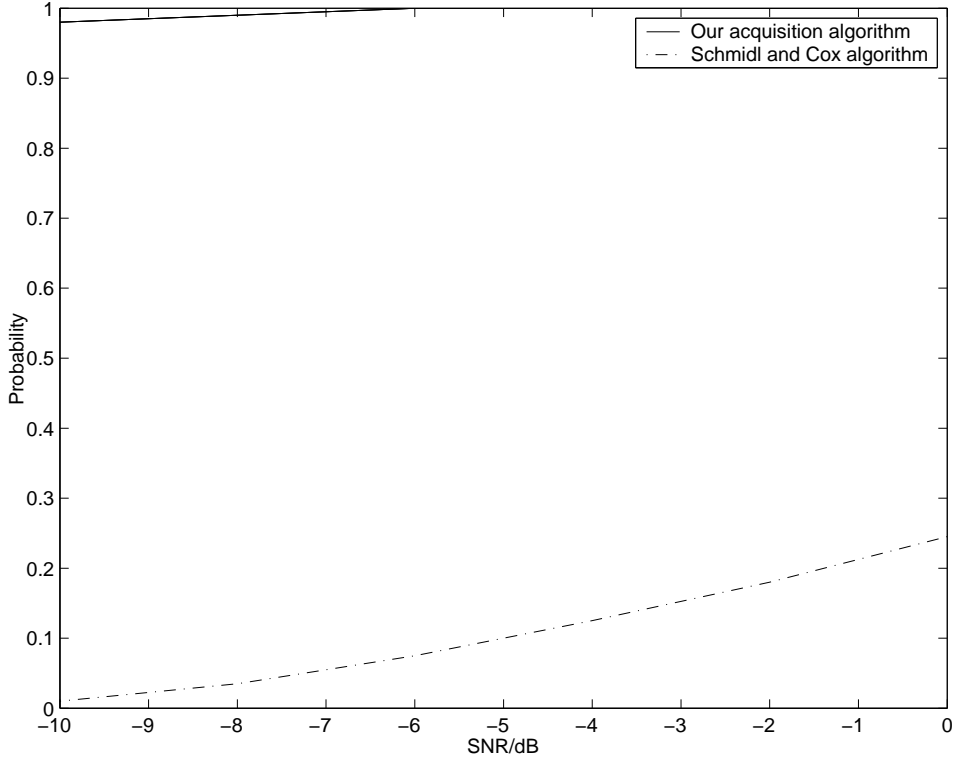

Figure 4.1: Comparison of the probability of correct synchronization of the proposed acquisition algorithm with Schmidl and Cox's for AWGN channel

In fig 4.1, we compare the probability of correct synchronization of the two algorithms. It can be easily seen that Schmidl and Cox's algorithm has poor timing synchronization performance in poor channel condition while our timing synchronization algorithm is unaffected by the value of SNR. This is mainly because in the proposed algorithm, the timing metric is a correlation of the received signal with the pilot. Due to the orthogonality of the OFDM

time samples and the property of white noise, the proposed timing metric will indicate the correct timing irrespective of the SNR value. Whereas for Schmidl and Cox's algorithm, they rely on the similarity of the 2 "long" training symbol to acquire the correct timing. At a SNR value lower than 0dB, the noise power is larger than the signal power. Thus the similarity of between the 2 "long" training symbols are destroyed by the noise. Hence the correlation provide little information about the correct timing.
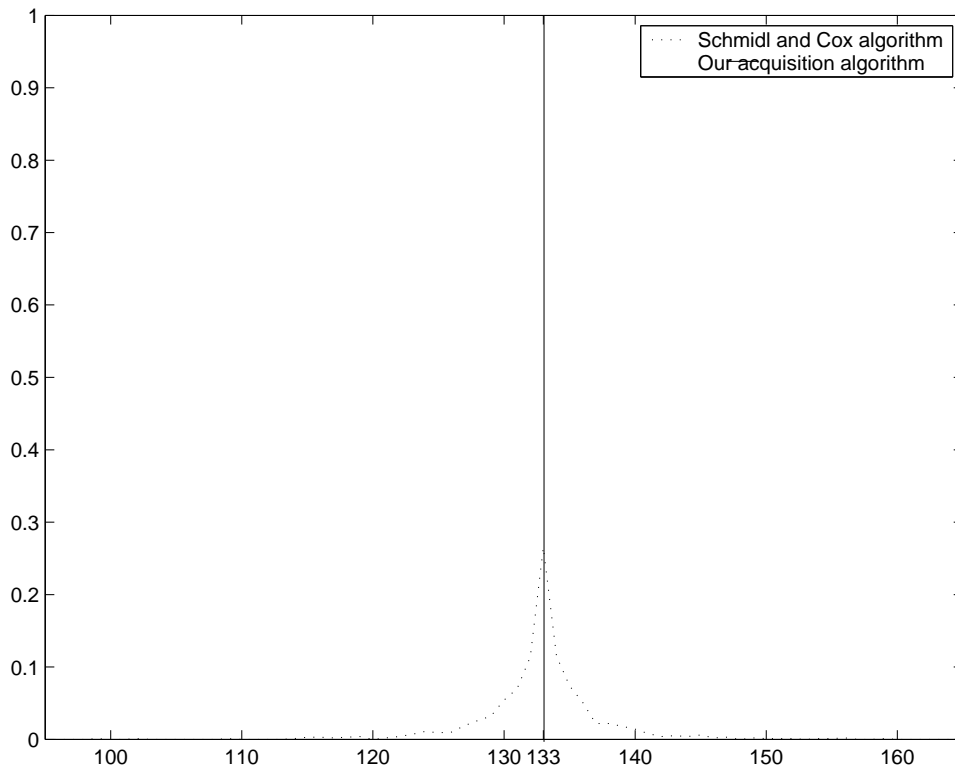

Figure 4.2: Comparison of the probability density function of the proposed acquisition algorithm with Schmidl and Cox's at 0dB for AWGN channel

The pdf of the two algorithms are compared in fig. 4.2. The pdf are generated at a SNR value of 0dB. It shows that while our proposed algorithm synchronize the receiver perfectly, the Schmidl and Cox's algorithm not only
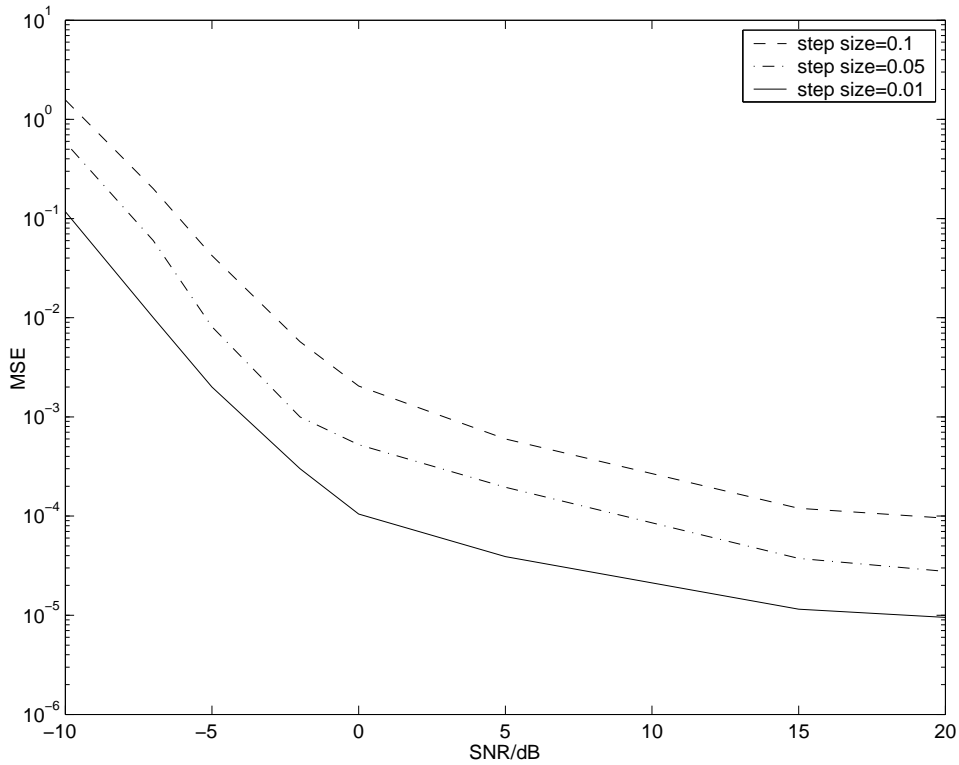
Figure 4.3: MSE of the proposed frequency estimator for AWGN channel

has low probability of correct synchronization but also has a large variance.

The mse of the frequency estimator is plotted in fig. 4.3 for different step size. As in adaptive algorithm, the step size has an effect of the performance and the computation complexity. The smaller the step size is, the better the mse performance but the more computation intensive it is. Furthermore the mse value saturates at high SNR. This is due to the finite step size value.

4.5.2 Performance in Multipath Fading Channel

We first illustrate how our proposed acquisition algorithm can handle multipath better. In fig. 4.4, the timing metrics used by the Schmidl and Cox algorithm are compared with both $|\gamma|$ and $|\beta|$ of our algorithm as defined respectively in Section 4.3 step 2 and 3. In particular, note that by coherently combining the contribution from each path, our algorithm correctly identify the arrival time of the first multipath component while Schmidl and Cox algorithm determines the position of synchronization as the maximum of the decision function (4.15), erroneously shifted from the correct position $i = 133$.
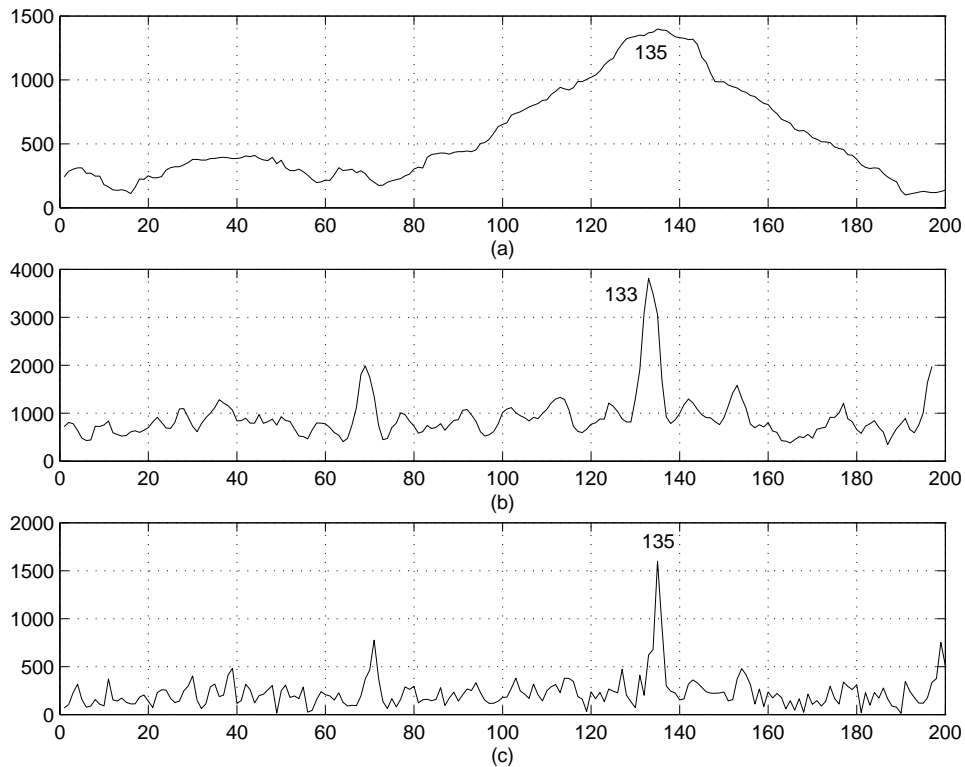

Figure 4.4: Timing metric value for SNR=20dB (a) Schmidl and Cox's algorithm [1] (b) proposed algorithm, $|\beta|$ (c) proposed algorithm, $|\gamma|$
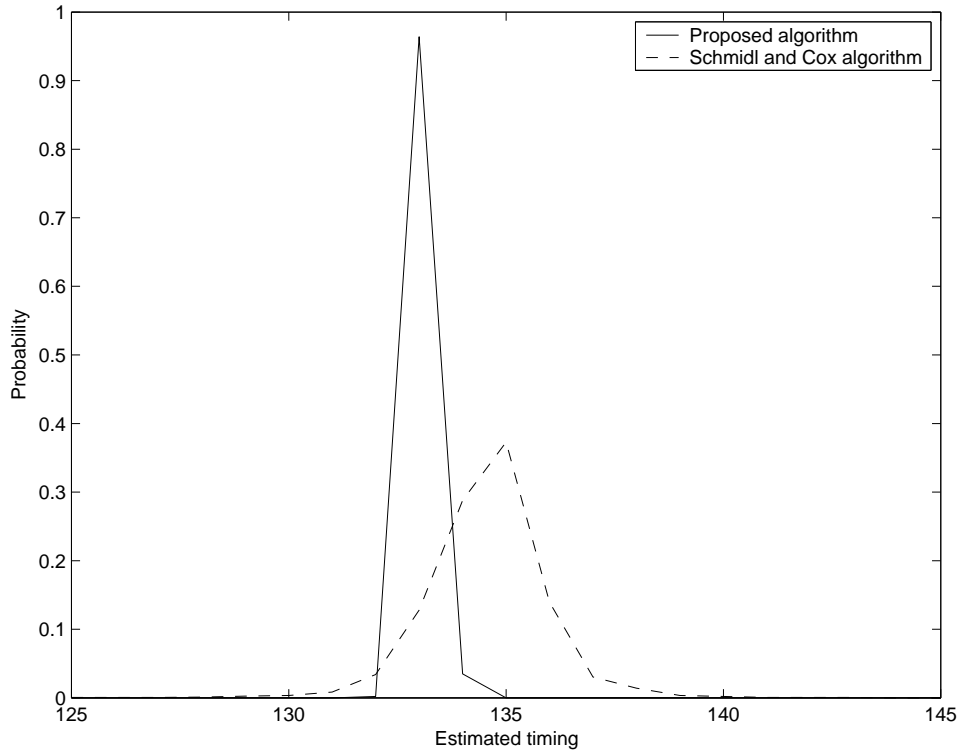
Figure 4.5: Comparison of the distribution of the timing estimate for proposed algorithm and Schmidl and Cox's algorithm [1]

The distribution of the timing estimate for two methods are shown in fig. 4.5. It can be seen that the distribution of our timing estimate peak at the correct position with high probability and small variance while the distribution of Schmidl and Cox timing estimate peak at the incorrect timing position. Particularly, our algorithm succeeded to recover the true timing exactly in more than 95% of the realizations, and to within a few sample intervals in other cases. For Schmidl and Cox algorithm, it only manages to recover the true timing exactly in less than 20% of the realizations, and to a wide range of sample intervals in other cases.

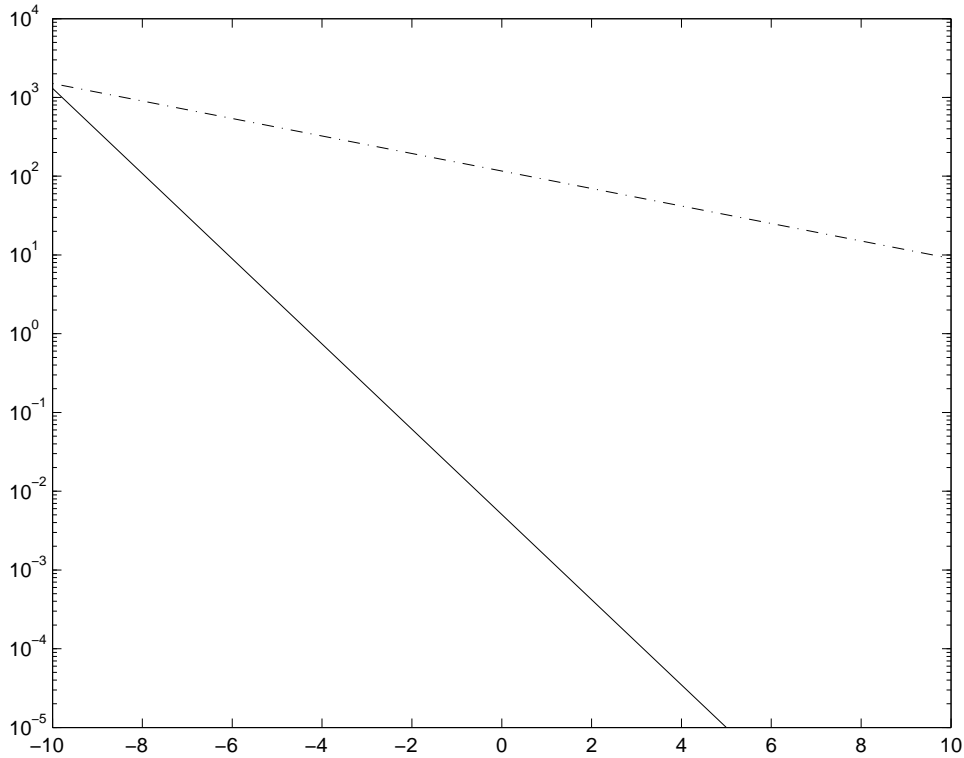Moreover, as shown in fig. 4.6, the mse value of Schmidl and Cox algo-

Figure 4.6: Comparison of the mse of the proposed acquisition synchronization algorithm with Schmidl and Cox's [1]

rithm is high and saturates for a SNR value of higher than 5dB. On the other hand, the mse value our proposed synchronization algorithm drops significantly with increasing SNR and becomes negligible for a SNR value of higher than 5dB. This implies our synchronization algorithm is both unbiased and consistent.

We then plotted the analytical probability of synchronizing to any path as defined in (4.13) in fig. 4.7. particularly, note that the analytical probability of synchronizing to any path matches well with the simulated probability of correct synchronization with perfect frequency offset estimation. Moreover, non perfect frequency offset estimation will degrade our synchro-
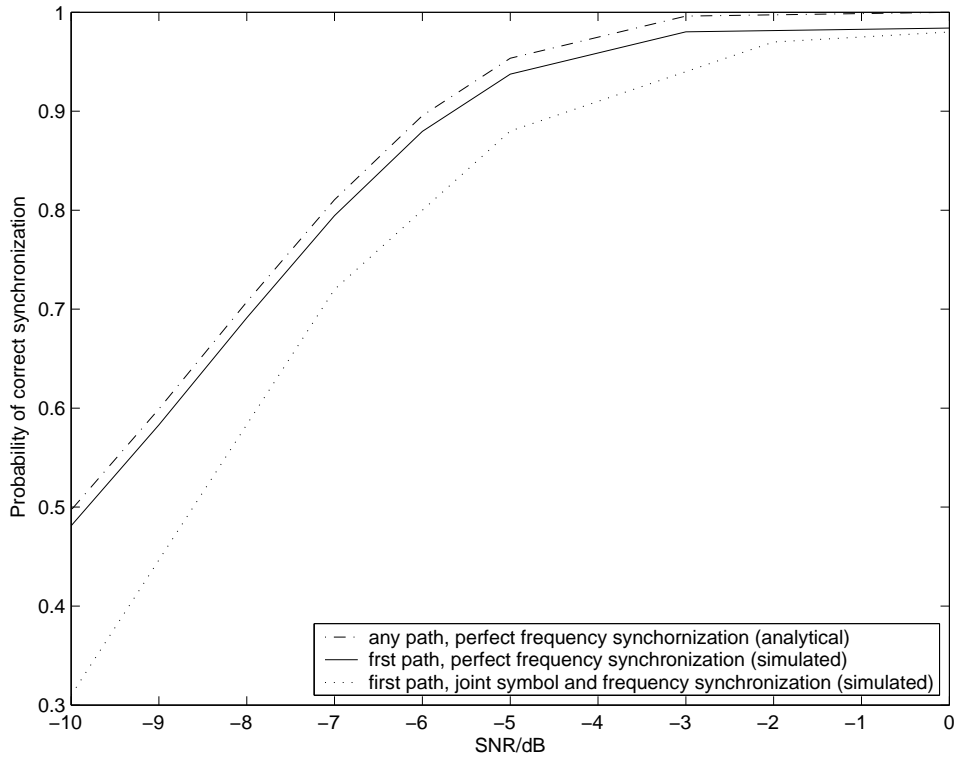
Figure 4.7: Comparison of the analytical and simulated probability of correct synchronization for our proposed algorithm

nization performance. However, the degradation becomes negligible for high SNR value. This is because at high SNR, the mse of our frequency offset estimation is low as shown in fig. 4.8. In fig. 4.8, a step size of 0.1, 0.05, 0.01 is considered. As discussed in Section 5.3.1, the mse value saturates at high SNR due to the finite step size value.

The analytical and simulated mean square error (MSE) of our channel estimation versus SNR is plotted in fig. 4.9. We show that both the analytical and the simulated mse value agree well.
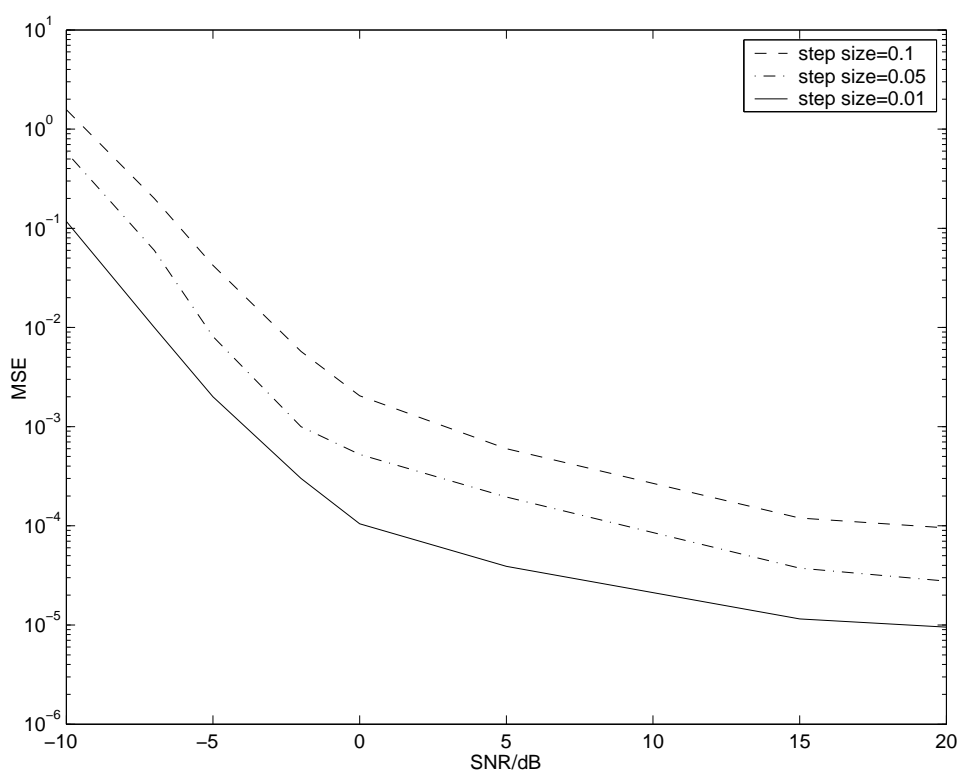
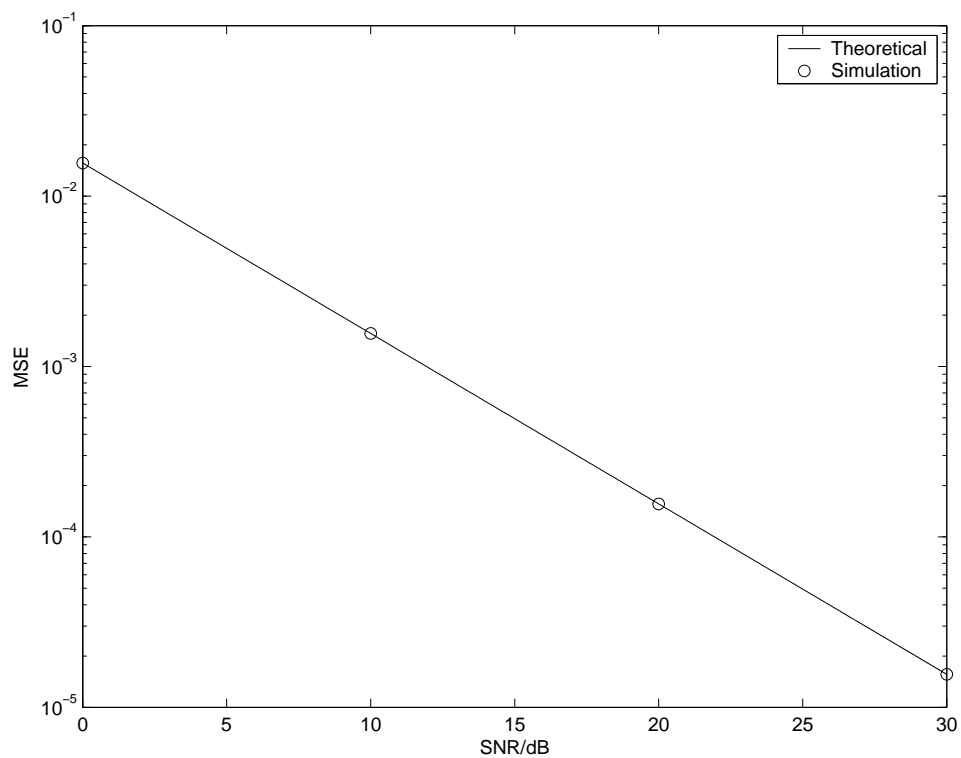Figure 4.8: MSE of the proposed frequency estimator

Figure 4.9: Comparison of simulated with analytical mean square error for our channel estimation algorithm

Chapter 5

Tracking Algorithm

In this chapter, the maximum-likelihood estimation function on which our tracking algorithm is based is derived. The tracking algorithm is formulated using the frequency pilot tones of the data carrying part. An analytical study of the performance was given.

5.1   ML Algorithm for Tracking

In this section, we deal with acquiring the estimates of the channel coefficients, h_i and the arrival time of the first multipath component, θ, using the frequency pilot tones in the data carrying part. Assume we transmit an OFDM symbol consisting of $N + L$ consecutive time samples, $s(k)$ starting from $s(0)$ and observe $N + N_m + L$ consecutive samples of $r(k)$ starting from $r(\theta)$. We then define $\mathbf{p} \triangleq [p(0), p(1), \ldots, p(N + L - 1)]^t$ as

the $(N + L) \times 1$ vector of the pilot part of the transmitted samples and $\mathbf{r} \triangleq [r(\theta), r(\theta + 1), \ldots, r(\theta + N + N_m + L - 1)]^t$ as the $(N + N_m + L) \times 1$ vector of the observed samples.

Due to the cyclic prefix, $\{r(k)|(\theta, \epsilon, \mathbf{h}, \mathbf{p})\}$ has mean

$$
\mu_k = \begin{cases} \sum_{l=0}^{k-\theta} h_l p(k - \theta - l) e^{\frac{j2\pi\epsilon k}{N}} & k \in A \\ \sum_{l=0}^{N_m-1} h_l p(k - \theta - l) e^{\frac{j2\pi\epsilon k}{N}} & k \in B \\ \sum_{l=k-\theta-M}^{N_m-1} h_l p(k - \theta - l) e^{\frac{j2\pi\epsilon k}{N}} & k \in C \end{cases} \tag{5.1}
$$

and a covariance structure of

$$
\begin{aligned}
c_{ab} = & E[r(a)r^*(b)|\mathbf{h}, \mathbf{p}, \theta, \epsilon] - \mu_a \mu_b^* \\
= & \begin{cases} \sum_{l=0}^{N_m-1} |h_l|^2 \sigma_m^2 + \sigma_n^2 & \forall \, a = b \\ \alpha_a \sigma_m^2 e^{-j2\pi\epsilon} & b = a + N, \ a \in D \\ 0 & elsewhere \end{cases} ,
\end{aligned}
$$

where

$$
\alpha_a = \begin{cases} \sum_{l=0}^{a-\theta} |h_l|^2 & a \in A \\ \sum_{l=0}^{N_m-1} |h_l|^2 & a \in B \\ \sum_{l=a-\theta-L}^{N_m-1} |h_l|^2 & a \in C \end{cases} ,
$$

$$
A = \{\theta, \theta + 1, \ldots, \theta + N_m - 1\},
$$
$$
B = \{\theta + N_m, \theta + N_m + 1, \ldots, \theta + M - 1\},
$$
$$
C = \{\theta + M, \theta + M + 1, \ldots, \theta + M + N_m - 1\},
$$
$$
D = \{\theta, \theta + 1, \ldots, \theta + N_m + L - 1\}.
$$

The log-likelihood function is then given by [18] as

$$\Lambda_t(\theta, \mathbf{h}) = \Lambda_{cp}(\theta, \mathbf{h}) + \Lambda_p(\theta, \mathbf{h}), \qquad (5.2)$$

where

$$
\begin{aligned}
\Lambda_{cp}(\theta, \epsilon, \mathbf{h}) &= \sum_{k=\theta}^{\theta+L+N_m-1} \log\left(\frac{f\{r(k), r(k+N)\}}{f\{r(k)\}f\{r(k+N)\}}\right) \\
&= -\sum_{k=\theta}^{\theta+L+N_m-1} \frac{\rho_k^2|y(k)|^2 + \rho_k^2|y(k+N)|^2}{\sigma_r^2(1-\rho_k^2)} \\
&\quad -\sum_{k=\theta}^{\theta+L+N_m-1} \frac{2\rho_k\Re\{y(k)y^*(k+N)e^{j2\pi\epsilon}\}}{\sigma_r^2(1-\rho_k^2)} \\
&\quad -\sum_{k=\theta}^{\theta+L+N_m-1} log(1-\rho_k^2), \qquad (5.3)
\end{aligned}
$$

$$
\begin{aligned}
\Lambda_p(\theta, \mathbf{h}) &= \sum_{k=\theta}^{\theta+M+N_m-1} \log\left(f\{r(k)\}\right) \\
&= -\sum_{k=\theta}^{\theta+M+N_m-1} \frac{|y(k)|^2}{\sigma_r^2}, \qquad (5.4)
\end{aligned}
$$

$$y(k) = r(k) - \mu_k,$$

$$\rho_k = \frac{\alpha_k\sigma_m^2}{\sigma_r^2},$$

$$\sigma_r^2 = \sum_{l=0}^{N_m-1} |h_l|^2\sigma_m^2 + \sigma_n^2.$$

Assume, ϵ has been estimated in the acquisition stage, θ can be estimated as

$$
\begin{aligned}
\hat{\theta}_{ML} = \arg\max\Bigg\{ &\sum_{k=\theta}^{\theta+L+N_m-1} \frac{2\rho_k\Re\{y(k)y^*(k+N)e^{j2\pi\epsilon} - |y(k)|^2 - |y(k+N)|^2\}}{(1-\rho_k^2)} \\
&-\sum_{k=\theta+L+N_m}^{\theta+N-1} |y(k)|^2 \Bigg\} \qquad (5.5)
\end{aligned}
$$

To estimate the channel coefficients, note that although h_i is complex, our log-likelihood function is real and concave. Applying the complex gradient operator proposed in [15], our channel estimate will be the solution of

$$\nabla^c_{h_i} \Lambda_t = 0$$

However, it is unfeasible to differentiate (5.2) which is the summation of (5.3) and (5.4) applying the complex gradient method proposed in [15] to obtain the optimal solution to estimate the channel coefficients, h_i. Instead, we can obtain sub-optimal solution of the channel estimates by differentiating (5.4). With that, we obtain

$$\hat{h}_i = \frac{1}{M\sigma_p^2} \sum_{k=\theta+i}^{\theta+M+i-1} r(k)p^*(k-\theta-i)e^{-\frac{j2\pi\epsilon k}{N}} \tag{5.6}$$

for $i = 0, 1, \ldots, N_m - 1$. The detail derivation is similar to Section 4.2 and is omitted here.

(5.6) shows that θ and ϵ are needed to estimate the channel coefficients while h_i are needed in (5.5) to estimate the timing offset. Thus, a logical problem arises. However, this can be solved if the tracking algorithm is followed by the acquisition algorithm in Section 4.2. If that's not the case, note that the channel estimator is a simple correlator similar to the acquisition algorithm in Section 4.2. Following the similar argument, the timing and frequency offset can be estimated as in the acquisition algorithm.

5.2 Tracking Algorithm

Using the results from Section 5.1, we now proposed a channel estimation and symbol synchronization algorithm that works in a multipath fading environment as below:

1. compute $\gamma(a, \hat{\epsilon}) = \frac{1}{M\sigma_p^2}\hat{\Phi}^H\mathbf{p}^H\mathbf{r}(a)$, This when expanded will be (5.6).

2. $\beta(a, \hat{\epsilon}) = \sum_{k=a}^{a+N_m-1} |\gamma(k, \hat{\epsilon})|$.

3. $\{\hat{\theta}, \hat{\epsilon}\} = \arg\{max\{\beta(a, \hat{\epsilon})\}\}$.

4. $\hat{h_0}, \hat{h_1}, \ldots, \hat{h}_{N_m-1} = \gamma(\hat{\theta}, \hat{\epsilon}), \gamma(\hat{\theta}+1, \hat{\epsilon}), \ldots, \gamma(\hat{\theta}+N_m-1, \hat{\epsilon})$.

5. Compute the timing metric in (5.5) and search for index that gives the maximum.

Firstly, we correlate our received samples with the phase shifted training symbol in the preamble. We vary the value of $\hat{\epsilon}$ in a fix step size from -1 to 1 for each i. Then, we coherently combine the contribution of the multipath such that we are always able to synchronize to the first arriving path even though it is not the strongest path. In step 3, we search for the arrival time of the first multipath component, $\hat{\theta}$ and the frequency offset, $\hat{\epsilon}$. Finally, we estimate the channel coefficients accordingly and compute the optimal timing and frequency offset.

5.3 Simulation Results and Discussion

In this section, the performance of the tracking algorithm is evaluated using computer simulation under simple AWGN channel and multipath Rayleigh fading channel. Particularly, mse value, pdf and probability of correct synchronization are used to evaluate the performance. We consider an OFDM system with N subcarriers where N_p subcarriers are used to transmit pilot information.

5.3.1 Performance in AWGN Channel

An AWGN channel can be modelled using (2.9) by letting $N_m = 1$ and $h_0 = 1$. Thus (5.5) can be modified accordingly as below to estimate θ:

1. $N_m = 0$

2. $\rho_k = \rho = \frac{\sigma_m^2}{\sigma_m^2 + \sigma_n^2}$

We first illustrate the probability of correct synchronization of the tracking algorithm in fig. 5.1 and in fig.5.2. SNR and N_p were varied and their effect on the probability of correct synchronization were observed. In fig. 5.1, it can be seen that for $N_p = 16$, the synchronization algorithm performs reasonably well. However, the tracking algorithm performs poorly for a small N_p value. This is due to the fact that the noise will have higher power than the pilot symbol. Thus all useful information are destroyed.

Moreover, as can be seen from fig. 5.2, the probability of correct synchronization is heavily dependent on the value of $\frac{N_p}{N}$. SNR has secondary effect
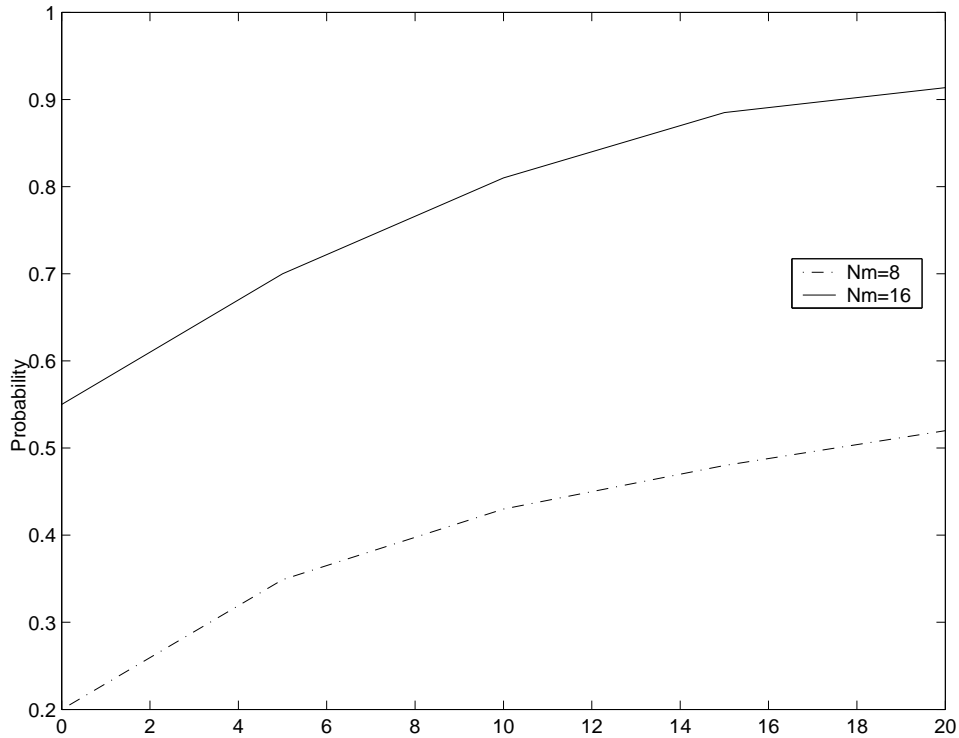
Figure 5.1: Probability of correct synchronization vs SNR

on the performance. Thus, by increasing $\frac{N_p}{N}$ value, we can achieve better synchronization performance. Furthermore in our derivation and simulation, we have assumed the power used to transmit the frequency pilot tones are the same as those used to transmit the data. Boosted pilots where the pilot tones power are increased such that it is larger than the noise power can be used to tackle this shortcoming. Fig. 5.2 indicates that when the ratio of pilot power to data power is greater than $1 : 3$, the algorithm synchronizes the receiver perfectly with a probability of above 0.9.

The mse of the synchronization algorithm are shown in fig.5.3 and fig. 5.4. It is noted that the mse saturates with increasing SNR value but de-

creases significantly with increasing $\frac{N_p}{N}$. This justifies that the value of $\frac{N_p}{N}$ has a huge influence on the synchronization performance while the influence of SNR is minor.

5.3.2 Performance in Multipath Fading Channel

We first illustrate the probability of correct synchronization of the tracking algorithm in fig. 5.5 and in fig.5.6. SNR and N_p were varied and their effect on the probability of correct synchronization were observed. In fig. 5.5, it can be seen that performs poorly in a multipath fading channel. This is due to the fact that the noise and intersymbol interference will have higher power than the pilot symbol. Thus all useful information are destroyed.

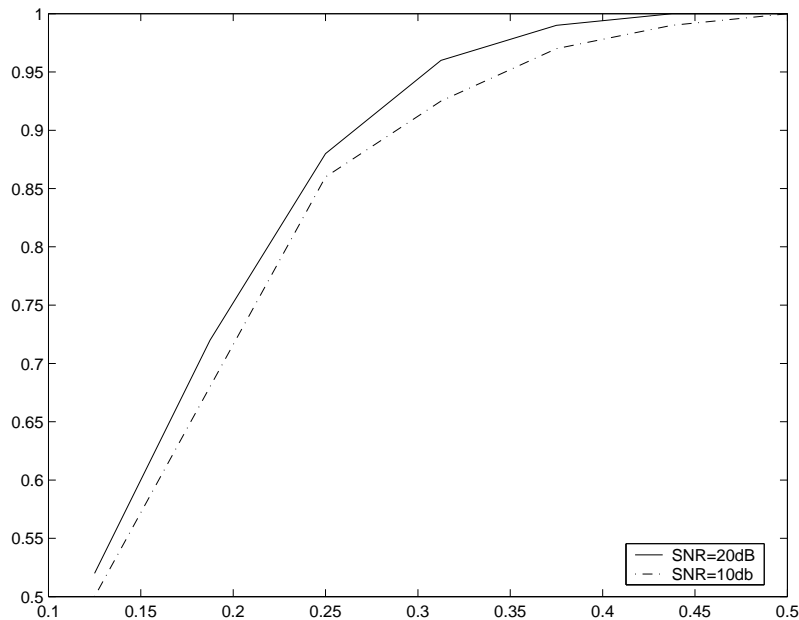However, as can be seen from fig. 5.6, the probability of correct synchro-

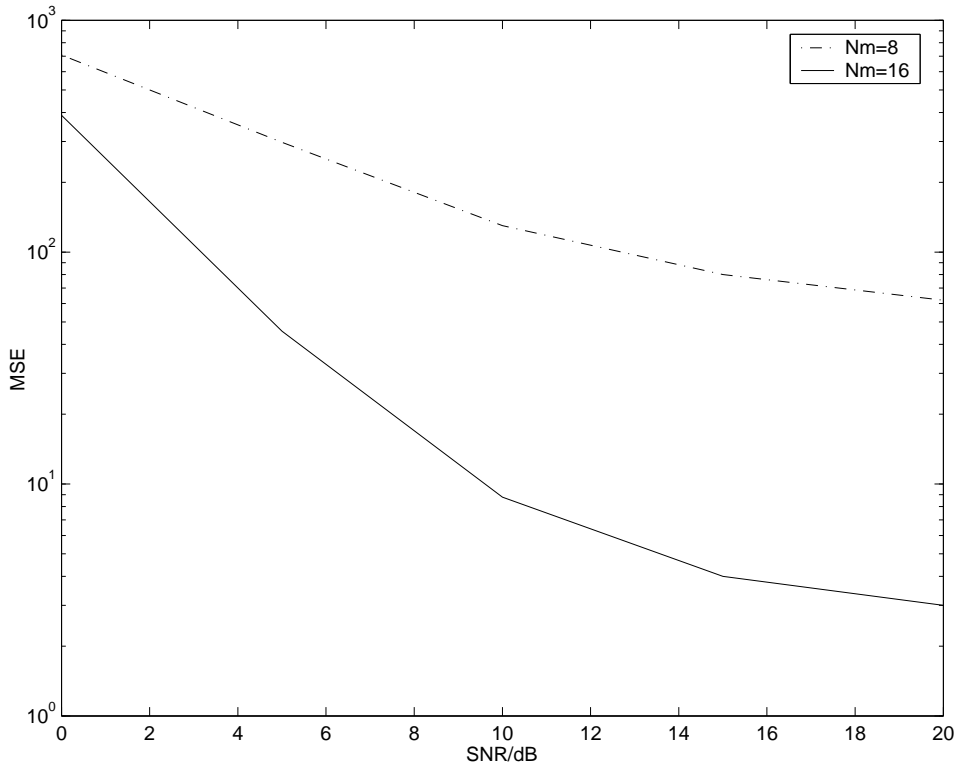**Figure 5.2: Probability of correct synchronization vs $\frac{N_p}{N}$**

Figure 5.3: MSE vs SNR

nization is heavily dependent on the value of $\frac{N_p}{N}$. SNR has secondary effect on the performance. Thus, by increasing $\frac{N_p}{N}$ value, we can achieve better synchronization performance. Furthermore in our derivation and simulation, we have assumed the power used to transmit the frequency pilot tones are the same as those used to transmit the data. Boosted pilots where the pilot tones power are increased such that it is larger than the noise power can be used to tackle this shortcoming. Fig. 5.6 indicates that when the ratio of pilot power to data power is greater than 1 : 2, the algorithm synchronizes the receiver perfectly with a probability of above 0.8.

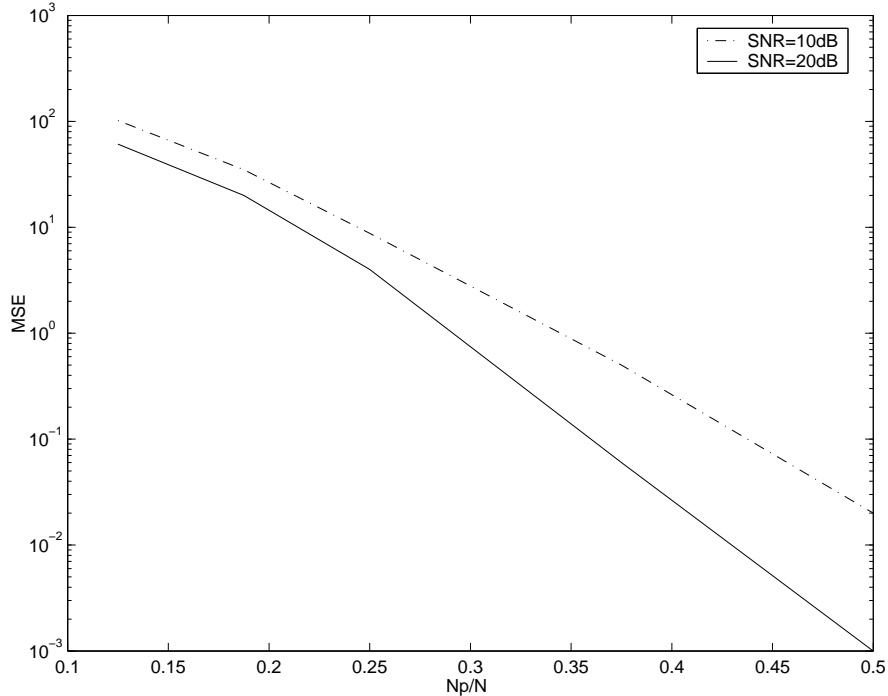The mse of the synchronization algorithm are shown in fig.5.7 and fig.

Figure 5.4: MSE vs $\frac{N_p}{N}$

5.8. It is noted that the mse saturates with increasing SNR value but decreases significantly with increasing $\frac{N_p}{N}$. This justifies that the value of $\frac{N_p}{N}$ has a huge influence on the synchronization performance while the influence of SNR is minor.

In fig. 5.9, we simulate the OFDM system considered above for a SNR value of 20dB to examine the convergence of our channel estimation algorithm. We show in fig. 5.9 that our channel estimator is unbiased as shown analytically. Particularly, note that our channel estimates converge to the true value within three hundreds OFDM symbols for an OFDM packet which usually consist of more than three thousands of OFDM symbols.
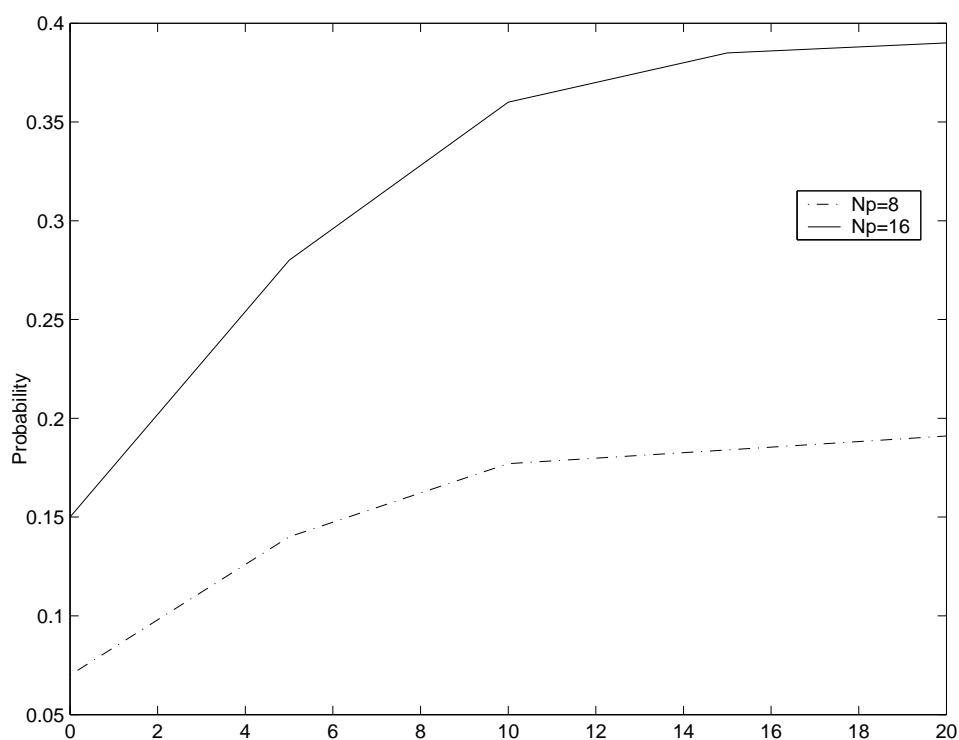
Figure 5.5: Probability of correct synchronization vs SNR

The analytical and simulated mean square error (MSE) of our channel estimation versus SNR is plotted in fig. 5.10. We show that both the analytical and the simulated mse value agree well.
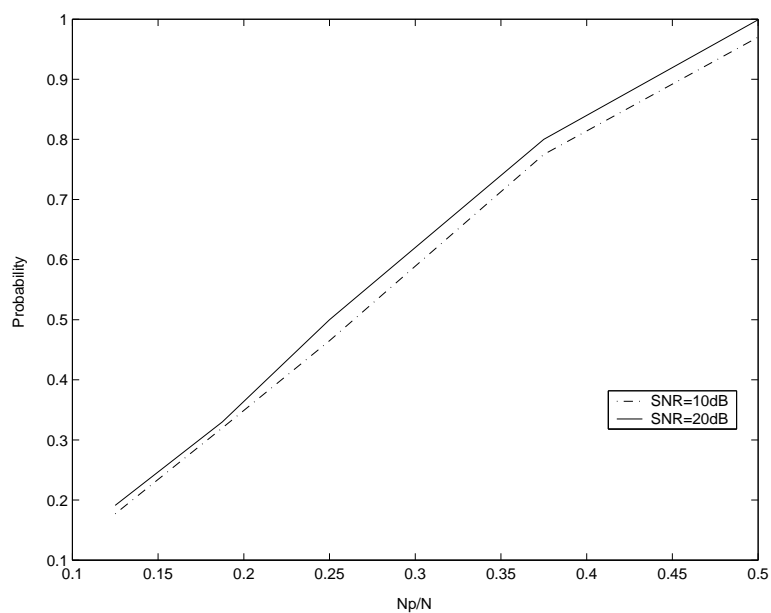
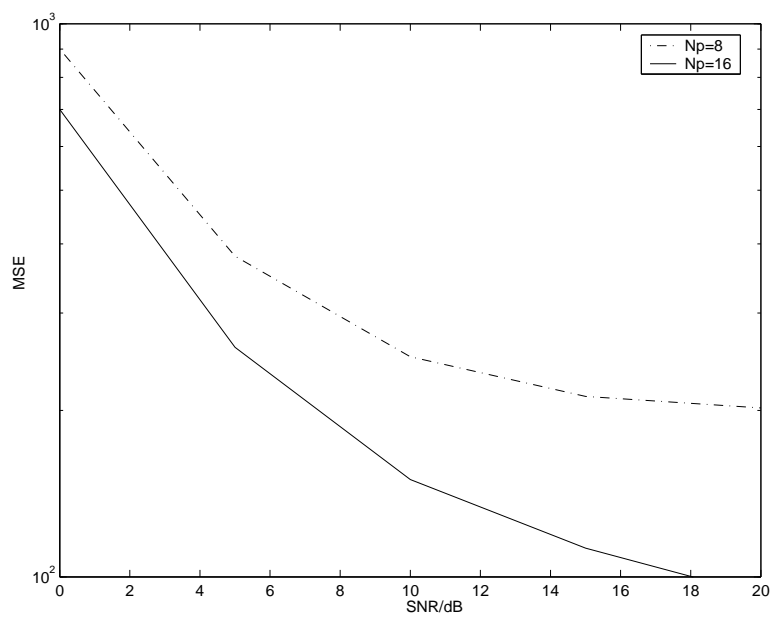Figure 5.6: Probability of correct synchronization vs $\frac{N_p}{N}$
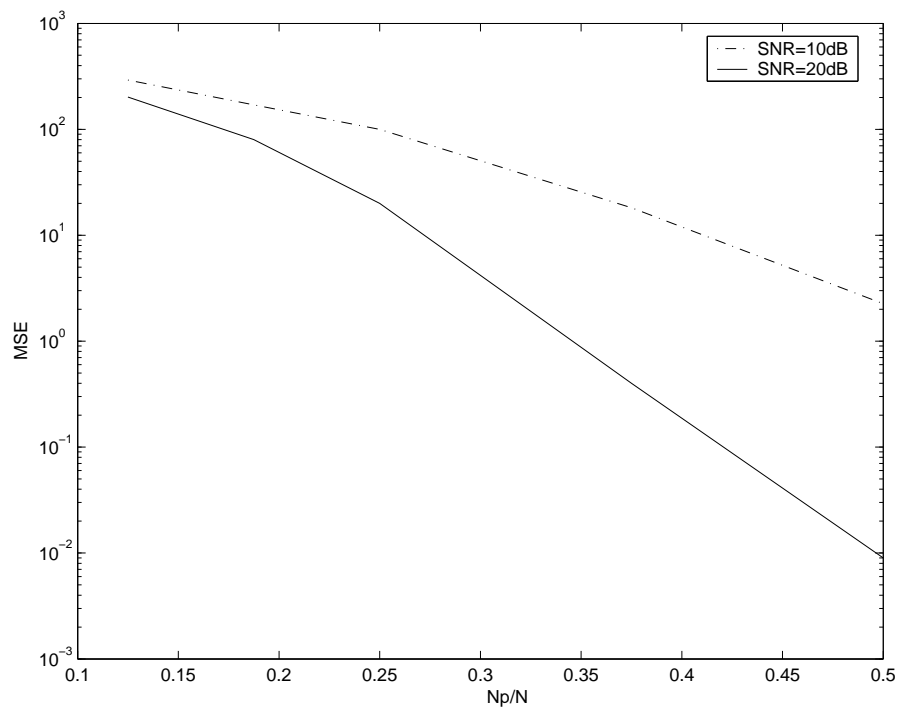

Figure 5.7: MSE vs SNR
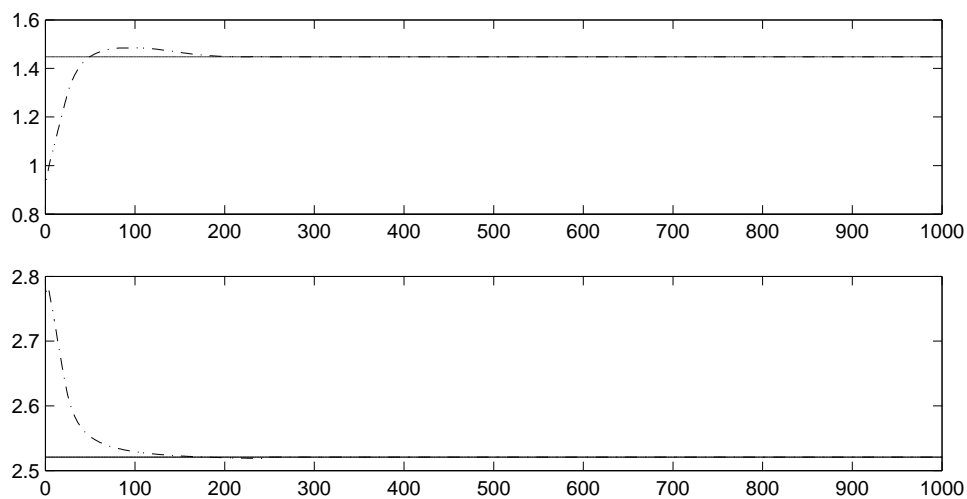
Figure 5.8: MSE vs $\frac{N_p}{N}$

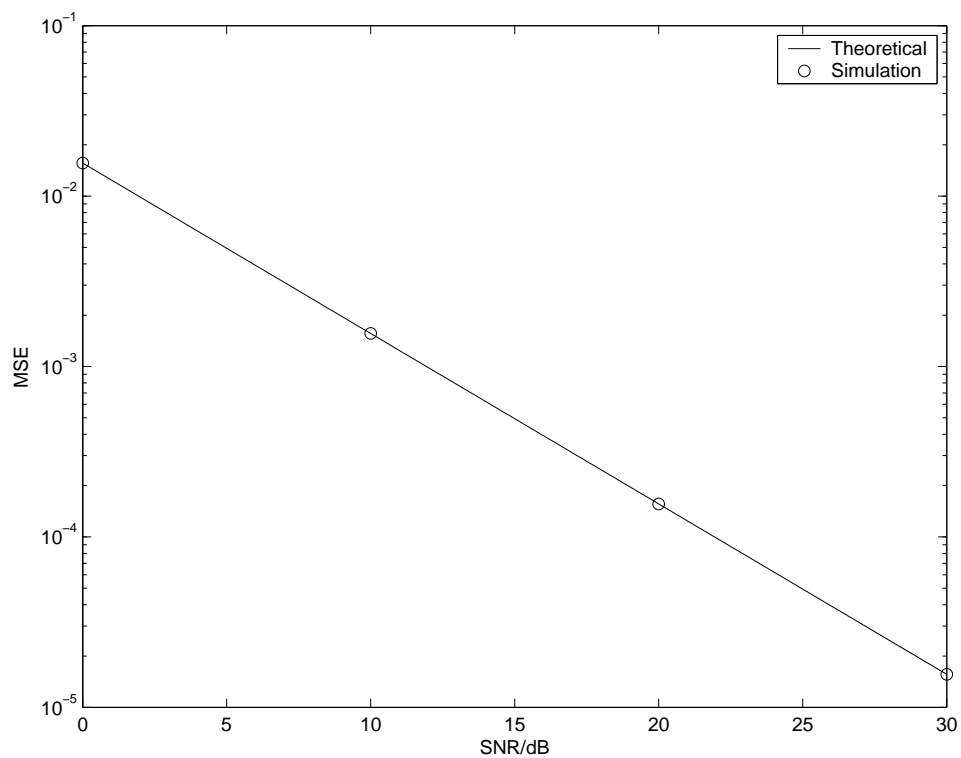Figure 5.9: Convergence analysis of our algorithm at SNR=20dB

Figure 5.10: Comparison of simulated with analytical mean square error for our channel estimation algorithm

Chapter 6

Conclusion and Future Topics

6.1 Conclusion

In this thesis, we have formulated a time domain joint channel estimation and synchronization algorithm for an OFDM system operating in multipath fading environment which complies with the IEEE 802.11a Wireless LAN standard. Both acquisition and tracking algorithm are addressed.

We introduced the OFDM packet as proposed in the IEEE 802.11a Wireless LAN standard in Chapter 2. A brief discussion on the fading channels follow and the received signal in the baseband is derived.

In chapter 3, we study the effect of frequency and timing offset. It is shown that frequency offset introduces ICI which severely degrades the system performance. For a offset value of between ± 0.5, it is noticed that a subcarrier barely interferes with its neighbour. Thus, it is argue that placement of null carriers is able to neutralize the effect of frequency offset.

A lower bound on the SIR is derived too. It is notice that the degradation is higher at high SNR value. The effect of timing offset is also examined. It is shown that there are 2 synchronization regions. At region A, the timing offset barely causes a rotation of phase of the data symbols which is not distinguishable with the rotation caused by the channel coefficients. The phase rotation is to be compensated by frequency domain equalizer.

In chapter 4, we first proved the orthogonality of OFDM time samples. We then presented the derivation of the acquisition algorithm. We applied the complex gradient method proposed in [15] to obtain the channel estimator. Due to the orthogonality of the time samples, we argue that we are able to extract frequency and timing offset information from the channel estimator. Noting this theoretical basis, we then proposed a systematic algorithm to acquire the estimates. Particularly, we coherently combine the contribution of each path to synchronize to the first arrival path. Analytical and simulation results show that our channel estimators are unbiased, consistence and efficient while an analytical expression of the probability of correct synchronization is derived too. Simulation results for both simple AWGN channel and a multipath fading channel show that the acquisition algorithm performs superbly even at very low SNR value.

In chapter 5, we derived the tracking algorithm. The likelihood estimation function is made up of 2 parts, the first due to the cyclic correlation while the second is a consequence of the pilot frequency tones transmitted in the data carrying part of the OFDM packets. We argue that it is unfeasible to differentiate the actual likelihood function to obtain the channel

estimates. Instead, we differentiate the part of the likelihood function intro-
duced by the frequency pilot tones. We obtain a similar channel estimator
as the acquisition algorithm which has similar properties of being unbiased,
consistent and efficient but with a higher MSE value. Simulation shows that
the synchronization performance depends on the $\frac{N_p}{N}$ value rather than SNR.
Thus, good synchronization performance can always be guaranteed regard-
less of SNR value as long as we are ready to transmit more pilot tones or
transmit the pilot information with higher power.

6.2 Suggestions for further works

The joint channel estimation and synchronization remains a challenging prob-
lem in the implementation of OFDM systems. In this thesis, we examine the
use of MLE which is pilot assisted with the orthogonality of the OFDM time
samples proved in Section 4.1.

Further studies can be done on the incorporation of MIMO technology
to into the system. A similar MLE estimation can be derived using an
approach similar to this thesis. In an OFDM system, some subcarriers may be
affected by the presence of channel nulls, rendering the subcarrier unsuitable
for data transmission. If information about the channel can be fed back to
the transmitter, the placement of subcarriers can be made adaptive so as to
maximize the overall system performance, which includes minimizing both
the channel and the synchronization estimation error.

Last but not least, the joint estimation in a multiuser system presents

a difficult task as each user has a different channel state information, timing and frequency offset. However, the deployment of such a multiuser system is highly desirable and this presents a potential research topic.

Bibliography

[1] T. M. Schmidl and D. C. Cox, "Robust frequency and timing synchro-
nization for OFDM," *IEEE Trans. Commun.*, vol. 45, pp. 1613–1621,
Dec. 1997.

[2] J. Proakis, *Digital Communications.* McGraw-Hill, 1989.

[3] R. Chang, "Synthesis of bandlimitted orthogonal signals for multichan-
nel data transmission," *BSTJ*, vol. 46, pp. 1775–1796, Dec 1966.

[4] M. Zimmermann and A. Kirsch, "The AN/GSC-10/KATHRYN/ vari-
able rate modem for hk radio," *IEEE Trans COmmun. Techn*, pp. 197–
205, April 167.

[5] S. Weinstein and P. Ebert, "Data transmission by frequency division
multiplexing using the discrete fourier transform," *IEEE Trans Commun
Techn*, vol. 19, pp. 628–634, Oct 1971.

[6] L. Cimini, "Analysis and simulation of a digital mobile channel using
orthogonal frequency division multiplexing," *IEEE Trans. Commun.*,
vol. 33, pp. 665–675, July 1985.

[7] *Radio Broadcasting Systems. Digital Audio Broadcasting DAB to mobile, portable and fixed receivers*, ETSI Std.

[8] *Digital Video Broadcasting DVB. DVB specification for data broadcasting*, ETSI Std.

[9] *Wireless LAN Medium Access Control (MAC) and Physical Layer(PHY)*, IEEE Std.

[10] B. Hirosaki, "An orthogonal multiplexed QAM system using the discrete fourier transform," *IEEE Trans. Commun.*, vol. 29, pp. 982–989, July 1981.

[11] Y. Wu and W. Y. Zhou, "Orthogonal frequency division multiplexing: a multicarrier modulation scheme," *IEEE Trans. Consumer Electronics*, vol. 41, pp. 392–398, Aug 1995.

[12] R. van Nee, G. Awater, M. Morikura, H. Takansashi, M. Webster, and K. Halford, "New high rate wireless LAN standards," *IEEE Commun. Mag.*, vol. 37, pp. 82–88, Dec. 1999.

[13] K. P. Ng, "Frequency offset estimation for orthogonal frequency division multiplexing," Master's thesis, National University of Singapore, 2003.

[14] P. Moose, "A technique for orthogonal freqeuncy division multiplexing frequency offset correction," *IEEE Trans. Commun.*, vol. 42, no. 10, pp. 2908–2914, October 1994.

[15] D. Brandwood, "A complex gradient operator and its applications in adaptive array theory," *Proc. IEEE*, vol. 130, pp. 11–16, Feb. 1983.

[16] M. Morelli and U. Mengali, "A comparison of pilot aided channel esti- mation methods for OFDM systems," *IEEE Trans. Signal Processing*, vol. 49, no. 12, pp. 3065–3073, Dec. 2001.

[17] E. Larsson, G.Liu, J. Li, and G. Giannakis, "Joint symbol timing and channel estimation for OFDM based WLANS," *IEEE Commun. Lett.*, vol. 5, pp. 325–327, Aug. 2001.

[18] J. van de Beek, M. Sandell, and P. Borjesson, "ML estimation of time and frequency offset in OFDM systems," *IEEE Trans. Signal Processing*, vol. 45, pp. 1800–1805, July 1999.

Appendix A

PDF of Timing Metric

We derive the pdf of our timing metric $|\gamma(a, \epsilon)|$ and $|\beta(a, \epsilon)|$ by assuming perfect frequency synchronization. Moreover, we drop the conditioning on $(\mathbf{h}, \mathbf{p}, \epsilon)$ for notational clarity.

$$
\begin{aligned}
\gamma(a, \epsilon) =& x_a + j y_a \\
=& \frac{1}{N_l \sigma_s^2} \sum_{k=0}^{N_l - 1} r(a + k) s^*(k) e^{\frac{-j 2\pi \epsilon k}{N}} \\
E[\gamma(a, \epsilon)] =& \frac{1}{N_l \sigma_s^2} \sum_{k=0}^{N_l - 1} E[r(a + k)] s^*(k) e^{\frac{-j 2\pi \epsilon k}{N}} \\
=& \begin{cases}
h_j & \text{if } 0 \leq j = a - \theta \leq N_m - 1 \\
h_{j-N} & \text{if } N \leq j = a - \theta \leq N + N_m - 1 \\
0 & \text{elsewhere}
\end{cases} \quad \text{(A.1)} \\
E[\gamma(a, \epsilon) \gamma^*(b, \epsilon)] =& \frac{1}{N_l^2 \sigma_s^4} \mathbf{p}^H \Phi^H E\{\mathbf{r}(a) \mathbf{r}^H(b)\} \Phi \mathbf{p} \\
=& \frac{1}{N_l^2 \sigma_s^4} \mathbf{p}^H \Phi^H E\{[\Phi \mathbf{S}(a) \mathbf{h} + \mathbf{n}(a)][\mathbf{h}^H \mathbf{S}^H(b) \Phi^H + \mathbf{n}(b)]\} \Phi \mathbf{p}
\end{aligned}
$$

$$= \frac{1}{N_l^2 \sigma_s^4} \mathbf{p}^H \mathbf{S}(a) \mathbf{h} \mathbf{h}^H \mathbf{S}^H(b) \mathbf{p} + \frac{1}{N_l^2 \sigma_s^4} \mathbf{p}^H \Phi^H E\{\mathbf{n}(a) \mathbf{n}^H(b)\} \Phi \mathbf{p}$$

$$= \begin{cases} |h_{a-\theta}|^2 + \frac{\sigma_n^2}{N_l \sigma_s^2} & a = b,\ a - \theta \in \{0, 1, \ldots, N_m - 1\} \\[1.5ex] \frac{\sigma_n^2}{N_l \sigma_s^2} & a = b,\ a - \theta \notin \{0, 1, \ldots, N_m - 1\} \\[1.5ex] |h_{a-\theta}|^2 & a + N = b,\ a - \theta \in \{0, 1, \ldots, N_m - 1\} \\[1.5ex] h_{a-\theta} h_{b-\theta}^* & a \neq b,\ \{a - \theta, b - \theta\} \in \{0, 1, \ldots, N_m - 1\} \\[1.5ex] 0 & \text{elsewhere} \end{cases}$$

$$\text{(A.2)}$$

Redo the above steps for $E[\gamma(a, \epsilon) \gamma(b, \epsilon)]$, we obtain

$$E[\gamma(a) \gamma(b)] = \begin{cases} h_{a-\theta}^2 & a = b,\ a - \theta \in \{0, 1, \ldots, N_m - 1\} \\[1.5ex] h_{a-\theta} h_{b-\theta} & a \neq b,\ \{a - \theta, b - \theta\} \in \{0, 1, \ldots, N_m - 1\} \\[1.5ex] h_{a-\theta}^2 & a + N = b,\ a - \theta \in \{0, 1, \ldots, N_m - 1\} \\[1.5ex] 0 & \text{elsewhere} \end{cases}$$

$$\text{(A.3)}$$

From (A.1),(A.2) and (A.3)

$$\mu_k = E[x_k] = \Re\{E[\gamma_k]\} \tag{A.4}$$

$$\eta_k = E[y_k] = \Im\{E\gamma_k]\} \tag{A.5}$$

$$E\{x_a x_b\} = \frac{1}{2}\{\Re\{E[\gamma(a)\gamma^*(b)]\} + \Re\{E[\gamma(a)\gamma(b)]\}\}$$

$$
= \begin{cases}
\frac{1}{2}\frac{\sigma_n^2}{N_l \sigma_s^2} + \Re\{h_{a-\theta}\}^2 & a = b, a - \theta \in \{0, 1, \dots, N_m - 1\} \\[2ex]
\frac{1}{2}\frac{\sigma_n^2}{N_l \sigma_s^2} & a = b, a - \theta \notin \{0, 1, \dots, N_m - 1\} \\[2ex]
\Re\{h_{a-\theta}\}\Re\{h_{b-\theta}\} & a \neq b, \{a - \theta, b - \theta\} \in \{0, 1, \dots, N_m - 1\} \\[2ex]
\Re\{h_{a-\theta}\}^2 & a + N = b, a - \theta \in \{0, 1, \dots, N_m - 1\} \\[2ex]
0 & \text{elsewhere}
\end{cases}
$$

$$
E\{x_a x_b\} - \mu_a \mu_b = \begin{cases}
\frac{1}{2}\frac{\sigma_n^2}{N_l \sigma_s^2} & a = b \\[2ex]
0 & a \neq b
\end{cases}
$$

$$
E\{y_a y_b\} = \frac{1}{2}\big\{\Re\{E[\gamma(a)\gamma^*(b)]\} - \Re\{E[\gamma(a)\gamma(b)]\}\big\}
$$

$$
= \begin{cases}
\frac{1}{2}\frac{\sigma_n^2}{N_l \sigma_s^2} + \Im\{h_{a-\theta}\}^2 & a = b, a - \theta \in \{0, 1, \dots, N_m - 1\} \\[2ex]
\frac{1}{2}\frac{\sigma_n^2}{N_l \sigma_s^2} & a = b, a - \theta \notin \{0, 1, \dots, N_m - 1\} \\[2ex]
\Im\{h_{a-\theta}\}\Im\{h_{b-\theta}\} & a \neq b, \{a - \theta, b - \theta\} \in \{0, 1, \dots, N_m - 1\} \\[2ex]
\Im\{h_{a-\theta}\}^2 & a + N = b, a - \theta \in \{0, 1, \dots, N_m - 1\} \\[2ex]
0 & \text{elsewhere}
\end{cases}
$$

$$
E\{y_a y_b\} - \eta_a \eta_b = \begin{cases}
\frac{1}{2}\frac{\sigma_n^2}{N_l \sigma_s^2} & a = b \\[2ex]
0 & a \neq b
\end{cases}
\tag{A.6}
$$

$$
E\{x_a y_b\} = \frac{1}{2}\big\{\Im\{E[\gamma(a)\gamma(b)]\} - \Im\{E[\gamma(a)\gamma^*(b)]\}\big\}
$$

$$
= \begin{cases}
\Re\{h_{a-\theta}\}\Im\{h_{a-\theta}\} & a = b, a - \theta \in \{0, 1, \dots, N_m - 1\} \\[2ex]
\Re\{h_{a-\theta}\}\Im\{h_{b-\theta}\} & a \neq b, \{a - \theta, b - \theta\} \in \{0, 1, \dots, N_m - 1\} \\[2ex]
\Re\{h_{a-\theta}\}\Im\{h_{a-\theta}\} & a + N = b, a - \theta \in \{0, 1, \dots, N_m - 1\} \\[2ex]
0 & \text{elsewhere}
\end{cases}
$$

$$
E\{x_a y_b\} - \mu_a \eta_b = 0 \tag{A.7}
$$

$$
E\{x_b y_a\} = \frac{1}{2}\big\{\Im\{E[\gamma(a)\gamma(b)]\} + \Im\{E[\gamma(a)\gamma^*(b)]\}\big\}
$$

$$= \begin{cases} \Im\{h_{a-\theta}\}\Re\{h_{a-\theta}\} & a = b, a - \theta \in \{0, 1, \ldots, N_m - 1\} \\ \Im\{h_{a-\theta}\}\Re\{h_{b-\theta}\} & a \neq b, \{a - \theta, b - \theta\} \in \{0, 1, \ldots, N_m - 1\} \\ \Im\{h_{a-\theta}\}\Re\{h_{a-\theta}\} & a + N = b, a - \theta \in \{0, 1, \ldots, N_m - 1\} \\ 0 & \text{elsewhere} \end{cases}$$

$$E\{y_a x_b\} - \eta_a \mu_b = 0 \tag{A.8}$$

From the autocovariance which is zero for different time instant and the cross-covariance which is always zero, x_k's and y_k's are statistically independent and hence $\gamma(k, \epsilon)$ are statistically independent too. Thus the joint pdf of x_k, y_k is

$$f(x_k, y_k) = \frac{1}{2\pi\sigma^2} \exp\left(-\frac{(x_k - \mu_k)^2 + (y_k - \eta_k)^2}{2\sigma^2}\right) \tag{A.9}$$

where

$$\sigma^2 = \frac{1}{2}\frac{1}{N_l}\frac{\sigma_n^2}{\sigma_s^2}.$$

By letting $z_k = |\gamma(k, \epsilon)|$ that is transforming (A.9) to polar coordinates and averaging over the angle, we obtain

$$f(z_k) = \begin{cases} \frac{z_k}{\sigma^2}\exp\left(-\frac{z_k^2}{2\sigma^2}\right) & \text{if } k \notin \{\theta, \theta+1, \ldots, \theta+N_m-1\} \\ \frac{z_k}{\sigma^2}\exp\left(-\frac{z_k^2+\mu_k^2+\eta_k^2}{2\sigma^2}\right)I_o\left(\frac{z_k\sqrt{\mu_k^2+\eta_k^2}}{\sigma^2}\right) & \text{if } k \in \{\theta, \theta+1, \ldots, \theta+N_m-1\} \end{cases} \tag{A.10}$$

Since $\beta(i, \epsilon) = \sum_{k=i}^{i+N_m-1} |\gamma(k, \epsilon)|$, β is Gaussian by CLT. The mean and

covariance of β are given by

$$E[\beta(i,\epsilon)] = \sum_{k=i}^{i+N_m-1} E[z_k]$$

$$R_{a,b} = E[\beta(a,\epsilon)\beta(b,\epsilon)] - E[\beta(a,\epsilon)]E[\beta(b,\epsilon)]$$

$$= \sum_{k=a}^{a+N_m-1}\sum_{m=b}^{b+N_m-1} E[z_k z_m] - E[z_k]E[z_m]$$

$$= \sum_{k=max(a,b)}^{min(a,b)+N_m-1} E[z_k^2] - E^2[z_k]$$

$$= \sum_{k=max(a,b)}^{min(a,b)+N_m-1} 2\sigma^2.$$

Thus, the joint pdf is given by

$$f\{\beta(1,\epsilon),\beta(2,\epsilon),\ldots,\beta(M,\epsilon)\} = \frac{1}{\sqrt{2\pi|R|}}exp\Big(-\beta'^t\mathbf{R}^{-1}\beta'\Big) \qquad (A.11)$$

where $\beta' = [\beta(1,\epsilon)-E\{\beta(1,\epsilon)\},\beta(2,\epsilon)-E\{\beta(2,\epsilon)\},\ldots,\beta(M,\epsilon)-E\{\beta(M,\epsilon)\}]^t$.

Appendix B

List of Publications

1. Wei Chee Lim,B Kannan,and T.T. Tjhung,"Channel and timing offset estimation for OFDM systems", *IEEE Trans. Signal Processing,* submitted for publication.

2. Wei Chee Lim, B Kannan,and T.T. Tjhung,"Joint channel and timing offset estimation for OFDM systems", to appear on *Int. Conf. Commun.* 04.